Tumour Marker Prognostic Study

INTERNATIONAL JOURNAL OF SURGERY

OPEN

Single-cell and bulk RNA-sequence identified fibroblasts signature and CD8 + T-cell - fibroblast subtype predicting prognosis and immune therapeutic response of bladder cancer, based on machine learning: bioinformatics multi-omics study

Jingxian Li, PhD[a], Zheng Kong, MS[a], Yuanjiong Qi, MD[a], Wei Wang, MS[a], Qiang Su, MS[a], Wei Huang, MS[a], Zhihong Zhang, MD[a,*], Shuai Li, MS[b,*], E Du, PhD[a,*]

Background: Cancer-associated fibroblasts (CAFs) are found in primary and advanced tumours. They are primarily involved in tumour progression through complex mechanisms with other types of cells in the tumour microenvironment. However, essential fibroblasts-related genes (FRG) in bladder cancer still need to be explored, and there is a shortage of an ideal predictive model or molecular subtype for the progression and immune therapeutic assessment for bladder cancer, especially muscular-invasive bladder cancer based on the FRG.

Materials and methods: CAF-related genes of bladder cancer were identified by analysing single-cell RNA sequence datasets, and bulk transcriptome datasets and gene signatures were used to characterize them. Then, 10 types of machine learning algorithms were utilised to determine the hallmark FRG and construct the FRG index (FRGI) and subtypes. Further molecular subtypes combined with CD8 + T-cells were established to predict the prognosis and immune therapy response.

Results: Fifty-four BLCA-related FRG were screened by large-scale scRNA-sequence datasets. The machine learning algorithm established a 3-genes FRGI. High FRGI represented a worse outcome. Then, FRGI combined clinical variables to construct a nomogram, which shows high predictive performance for the prognosis of bladder cancer. Furthermore, the BLCA datasets were separated into two subtypes – fibroblast hot and cold types. In five independent BLCA cohorts, the fibroblast hot type showed worse outcomes than the cold type. Multiple cancer-related hallmark pathways are distinctively enriched in these two types. In addition, high FRGI or fibroblast hot type shows a worse immune therapeutic response. Then, four subtypes called CD8-FRG subtypes were established under the combination of FRG signature and activity of CD8 + T-cells, which turned out to be effective in predicting the prognosis and immune therapeutic response of bladder cancer in multiple independent datasets. Pathway enrichment analysis, multiple gene signatures, and epigenetic alteration characterize the CD8-FRG subtypes and provide a potential combination strategy method against bladder cancer.

Conclusions: In summary, the authors established a novel FRGI and CD8-FRG subtype by large-scale datasets and organised analyses, which could accurately predict clinical outcomes and immune therapeutic response of BLCA after surgery.

Keywords: bladder cancer, clinical prognosis model, fibroblasts, immune infiltration, immune therapy

[a]Tianjin Institute of Urology, The Second Hospital of Tianjin Medical University and [b]Department of Colorectal Surgery, The Second Hospital of Tianjin Medical University, Tianjin, People's Republic of China

Jingxian Li, Zheng Kong, Yuanjiong Qi, and Wei Wang contribute equal to this article.

Sponsorships or competing interests that may be relevant to content are disclosed at the end of this article.

**Corresponding authors. Address: Tianjin Institute of Urology, The Second Hospital of Tianjin Medical University. Pingjiang Road 23#, Hexi District, Tianjin 300211, China. Tel.: +86 228 832 8695. E-mail: duedoc@tmu.edu.cn (E Du), and E-mail: zhangzhihongtianj@163.com (Z. Zhang); Department of Colorectal Surgery, The Second Hospital of Tianjin Medical University. Pingjiang Road 23#, Hexi District, Tianjin 300211, China. Tel.: +86 228 832 8695. E-mail: drlishuai@163.com (S. Li).*

International Journal of Surgery (2024) 110:4911–4931

Received 6 February 2024; Accepted 14 April 2024

Supplemental Digital Content is available for this article. Direct URL citations are provided in the HTML and PDF versions of this article on the journal's website, www.lww.com/international-journal-of-surgery.

Published online 17 May 2024

http://dx.doi.org/10.1097/JS9.0000000000001516

Instruction

Bladder cancer is one of the most common urological malignancies all over the world, with ~549 000 new cases and up to nearly 20 000 deaths per year[1], which is characterised by prevalence, high risk of recurrence, and treatment failures[1–3]. Bladder cancer is mainly classed as nonmuscle invasive bladder cancer (NMIBC), muscle-invasive bladder cancer (MIBC), and metastatic bladder cancer[4]. For MIBC, radical removal of the bladder with concomitant meticulous pelvic lymph node dissection has become the gold standard way for many decades. Despite this, the majority of patients recur with metastases, and half of them die within 5 years[5]. Multimodal treatment involving radical cystectomy (RC) with neoadjuvant chemotherapy provides the best opportunity against BLCA. In addition, advanced cancer is mainly first received systemic cisplatin-based chemotherapy as well as immunotherapy when the first-line therapy comes into failure[4]. However, a third of patients treated with NAC prove to be nonresponders who have a worse outcome than responders[6]. Immune checkpoint inhibitors targeting PD1 and PD-L1 are novel systemic therapies for BLCA, especially metastatic BLCA, for patients who are ineligible for cisplatin-based chemotherapy. However, the patients revealed diverse clinical responses, and the objective response rate was low in treating immune therapy single for metastatic BLCA (6% complete response, 17% partial complete, 25% stable disease, and 37% progressive disease)[7]. Recent developments have shed interesting light on molecular subtypes of bladder cancer that might differ from one another in response to various treatments[8,9]. However, no diagnostic markers represent consistent clinical utility; as the EAU MIBC guidelines put it, 'There is still destitute of evidence to utilise molecular subtypes, immune or other gene expression signature for characterizing, and managing MIBC patients'[10]. Therefore, developing practical molecular markers and subtypes for BLCA to provide a choice of therapeutic strategy is necessary and emergent.

As the major element in TME, fibroblasts have been widely studied and reported to participate in multiple biological functions, such as cell differentiation, proliferation, stemness, migration, and apoptosis. Generally speaking, fibroblasts are referred to as the most versatile and resilient cells that function in the maintenance of tissue structure and wound healing processes[11,12]. Under normal physiological circumstances, quiescent fibroblasts could be reversibly activated to repair and regenerate damaged tissues[13]. Intriguingly, activated fibroblasts will be restored to the previous phenotype when the wound heals, revealing that reversibility is a hallmark feature of fibroblasts-related to the repair of tissue[14]. In the light of cancer, an irreversible transition occurs in fibroblasts in many ways, and the cancer-associated phenotypes emerge, which changes the normal fibroblasts to cancer-associated fibroblasts (CAFs)[15,16]. CAFs are simply considered fibroblasts that situate within or adjacent to a tumour, which has long been considered to be a factor of protumour through various manners and signalling pathways. For example, the fibroblasts-mediated TGF-β pathway contributes to cancer cell proliferation, invasion, migration, and metastasis by secreting multiple growth factors[17]. Many studies about P13K/AKT signalling pathways in CAFs have revealed that activating this axis could induce cancer malignant behaviour, such as cell proliferation[18–20]. CAF-derived epiregulin could facilitate cancer cell proliferation through a downstream effector of MAPK signalling, which could be counteracted by ERK inhibitors U0126 and PD98-59[21,22]. Except for pathways mentioned above, CAFs could promote cancer progression by regulating JAK-STAT, NF-κB, Hippo, Notch, Hedgehog, and HIF-1α signalling cascades[23–29]. All these signalling hubs in CAFs have promising potential as targets to block the link between CAFs and cancer. In addition, CAFs have been found to relate to other cells from the tumour microenvironment (TME) to favour malignant biological behaviours and immunosuppression. As it did in the case of CD70 in CAFs, which could affect the T lymphocytes' differentiation by triggering the NF-κB signalling pathway[30]. CAFs-derived presenilin1 could regulate tumour-infiltration lymphocyte populations in the TME, which IL-1β could inhibit to promote activation of CD8 + T-cells to improve the efficacy of immune therapy[31]. The angiotensin receptor blocker losartan cancer reduces CAFs into a quiescent state, reverses immunosuppression, and activates T lymphocytes[32]. Apparently, targeting all sorts of pathways could change the regulation of CAFs to immune cells and affect the response of tumour to the immune system and therapy. CAFs have also been found to be associated with therapeutic resistance. The interaction between tumour cells and CAFs blunts the response of tumour cells to chemotherapy, targeted therapy, and radiotherapy[33]. CAFs could be stimulated by drugs in chemotherapy-activated tumour stemness and enhance treatment resistance by facilitating multiple pathways or secreting cell factors[29,34]. Similarly, a combination of CAFs and tumours could reduce the effects of small molecule drugs against tumours[35]. In addition, the generation of the hypoxic microenvironment and the EMT signalling activation forced by CAFs also defend radioresistance to cancer cells[36,37]. All in all, CAFs regulate tumour behaviour not only by mediating multiple cancer-associated hallmark pathways but also by affecting the immune system and response to all sorts of therapies. Compared to other cancers, CAFs have been studied less extensively in BLCA. However, there is still some evidence revealing that CAFs could be associated with BLCA malignant phenotypes and could be predictors of response to BLCA therapies. For instance, BLCA patients with high fractions of SLC14A1 + CAFs represented poor outcomes and a worse response rate to NAC and immune therapy, which is induced by interferon signalling and the WNT paracrine pathway[38]. Another study stated that CAF-derived miR-146a-5p could induce BLCA stemness and chemoresistance by producing a niche[39]. CAF also can weaken the immune cell infiltration in bladder cancer and facilitate immune escape by up-regulating PD1/PD-L1[40]. However, the crosstalk between CAFs and BLCA cells has not been established, and it remains underexplored and worthy of additional excavation. For other novel therapies, including enfortumab vedotin (EV), sacituzumab govitecan, and RC48, antibody-drug conjugates targeting

HIGHLIGHTS

- We established a fibroblast-related genes index (FRGI) and novel fibroblast-CD8 + T-cells subtype to predict prognosis and immune therapeutic response in bladder cancer.
- The subtype provided a comprehensive therapeutic strategy for bladder cancer patients based on different mechanisms, immune systems, and epigenetic characteristics.
- Further well-designed preclinical and clinical trials are necessary to obtain conclusive results.

NECTIN4, TROP-2, and ERBB2, respectively, there are no reports yet on the putative relevance of CAFs in the case of this treatment. These results tipped that targeting CAFs is a promising therapeutic strategy against BLCA. However, further exploration of CAFs on BLCA by preclinical and clinical experiments is still needed in the future.

So far, there is no single biomarker that could be used to identify CAFs. Long before, α-smooth muscle actin (αSMA) was referred to as an ideal marker to identify fibroblast[41]. However, subsequent research proved that it is oversimplified because many biomarkers have been determined[42,43]. Recent research has established multiple models or subtypes based on CAFs to predict the prognosis and immune therapy response of patients with BLCA[44–46]. However, most of them ignored the role of CAFs in regulating immune cells in TME. In this study, we aimed to identify several specific biomarkers of fibroblast and established FRG index (FRGI) to predict prognosis in BLCA. We also considered the role of immune cells in TME and combined CD8 + T-cells with the FRG signature to stratify the patients with BLCA exactly to predict prognosis and immune therapeutic response. Pathways enrichment analysis and epigenetic alteration are performed to provide a comprehensive strategy for further combination therapy based on FRG subtypes.

Result

Identification of fibroblast-related genes (FRG) in bladder cancer

To explore stage-related components of the TME in bladder cancer, we first clustered a single-cell RNA sequence dataset of bladder cancer (Fig. 1A). Shortly afterwards, the clusters were further annotated by SingleR R-package (Fig. 1B). We found immune cells (such as DC, Monocyte, and Macrophage), fibroblast, and endothelial cells pointed to a correlation with bladder cancer T stage, that is, a higher proportion of these cells accompanied with advanced stage. A great deal of research has pointed out a close relationship between fibroblasts and tumour progression and immune suppression, thus forcing us to focus on this sort of cells in bladder cancer. Through the filtering threshold set previously, we further identified fibroblast-related genes based on the scRNA dataset - GSE135337 (Fig. 1C, Table S2, Supplemental Digital Content 1, http://links.lww.com/JS9/C615). To validate these genes, we had them as a gene set and submitted them to the public scRNA website - TISCH. The weighted average value of mRNA expression of these genes was cast on another BLCA scRNA-seq dataset - GSE130001, and the result revealed that these genes were highly enriched in the fibroblast cluster (Fig. 1D and E). The same analyses were further conducted in other scRNA-seq datasets across pan-cancer and showed universally similar results; that is, high enrichment of these genes was observed on clusters representing fibroblasts in TME (Fig. S1A and B, Supplemental Digital Content 2, http://links.lww.com/JS9/C616). Interestingly, the concordance rate (i.e. the number of differential expression FRG in other scRNA-seq datasets/54 identified FRG in GSE135337) of differential expression FRG was highest in bladder cancer, indicating that several FRG were peculiarly expressed in BLCA. Of course, identified FRG were also observed expression upregulation in several other cancer types, such as BCC, BRCA, CHOL, CRC, STAD, SKCM, and STAD, indicating these FRG signatures could extend to other cancers (Fig. S1C, Supplemental Digital Content 2, http://links.lww.com/JS9/C616). To identify whether these genes express in or highly correlate with fibroblast, we further calculated the correlation between these genes and other identified signatures - Fges[47], xCell[48], MCP counter[49] in TCGA-BLCA datasets and two pan-cancer cohorts (TCGA-Pan-cancer and GSE2109) (Fig. 1F, Fig. S2A and B, Supplemental Digital Content 2, http://links.lww.com/JS9/C616). Most genes show a highly positive correlation with fibroblasts and other stroma-derived signatures. Intriguingly, these genes showed a low correlation or negative correlation with immune-related cells, such as CD8 + T-cells, NKT, and CD4 + Tcm. These results further demonstrated that these genes could be referred to as a fibroblast signature in bladder cancer and even pan-cancer. Further protein-protein interaction (PPI) analysis revealed that these genes closely interacted with each other (Fig. S2C, Supplemental Digital Content 2, http://links.lww.com/JS9/C616). FN1 possesses the highest amount of collected nodes with other genes, indicating that FN1 might act as a core gene among this signature in fibroblasts. Co-expression analysis revealed that most genes highly correlated with others, but CXCL14, PLAT, and RGS5 seem to have a lower correlation with other genes in bladder cancer (Fig. S2D, Supplemental Digital Content 2, http://links.lww.com/JS9/C616). All in all, these identified genes could be referred to as fibroblasts' signatures to subsequent research in bladder cancer.

Epigenetics alteration and mechanism of FRG in bladder cancer

We then conducted a differential expression analysis. The results revealed that most genes showed a down-regulation in bladder cancer (Fig. 2A), whereas SERPINH1 and CTHRC1 showed a slight upregulation in cancer. In bladder cancer tissues, we observed that these genes are mainly expressed in stroma, illustrating they are not derived from tumour cells (Fig. 2B and Fig. S3, Supplemental Digital Content 2, http://links.lww.com/JS9/C616). Mechanically speaking, these genes are mainly enriched in focal adhesion, vascular smooth muscle contraction, proteoglycans in cancer, protein digestion and absorption-related pathways, identical protein binding, extracellular matrix structural constituent, receptor binding-related molecular functions, located in extracellular regions (Fig. 2C, Table S3, Supplemental Digital Content 3, http://links.lww.com/JS9/C617). In addition, these genes might be associated with several biological progressions, such as cell adhesion, response to hypoxia, and angiogenesis. In the mutation profile, the mutation rate of these FRG is low, but COL6A3 and FN1 show a mutation rate $> 5\%$ but $<10\%$ (Fig. 2D), indicating that mutation plays a faint role in these gene expressions. We then focus on copy number variation (CNV). The CNV gain and loss of FRG are frequent in bladder cancer. However, only IFITM3 and IFITM2, which show a higher number of CNV loss, showed a moderate correlation with their mRNA expression, demonstrating that these two gene expressions might be controlled by their CNV to some degrees (Fig. 2E, Fig. S4A, Supplemental Digital Content 2, http://links.lww.com/JS9/C616). We further analysed the DNA methylation of FRG and found that methylation levels of several genes in the specific methylation site showed a differential expression (Fig. 2F). Interestingly, most sites with down-regulated methylation levels showed a positive correlation with corresponding gene mRNA expression. These positive correlation

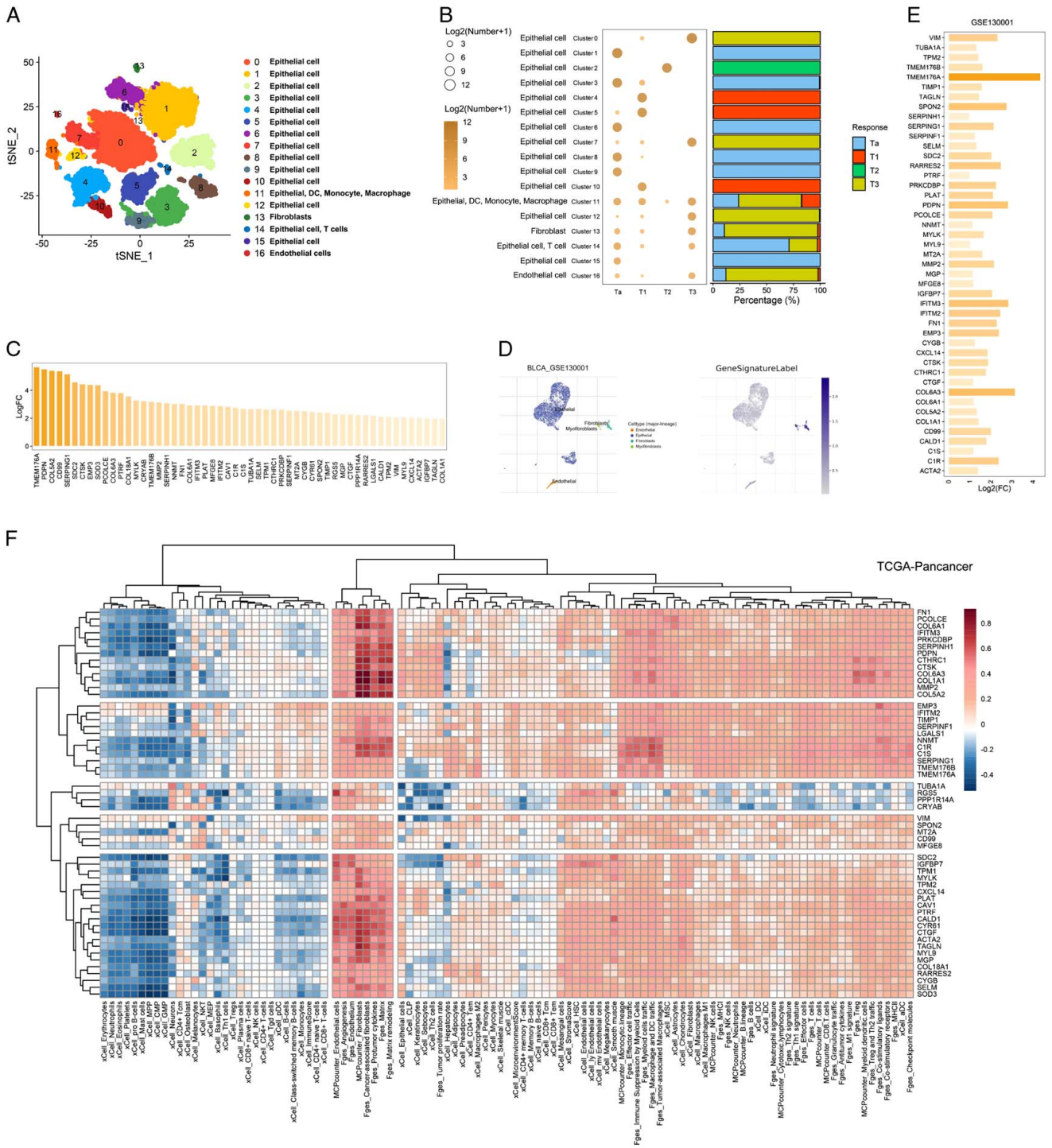

Figure 1. Determination of fibroblast-related genes (FRG). (A) t-SNE shows 16 clusters representing different cells in the tumour microenvironment. (B) Number and proportion distribution of different cluster cells in gradually advanced pathological T stage. (C) Barplot represents the log2 Fold Change (logFC) of identified FRG in the BLCA dataset - GSE135337. (D) Identified FRG was submitted to TISCH website to validate expression distribution in the GSE130001 dataset. (E) Barplot shows the log2 Fold Change (logFC) of identified FRG in the BLCA dataset - GSE130001. (F) The score of each gene set representing different TME signatures was calculated in the TCGA-pan-cancer dataset, and then the Pearson correlation coefficient between gene signature score and FRG expression was computed and then depicted by heatmap. The red represents a positive correlation, and the blue represents a negative correlation.

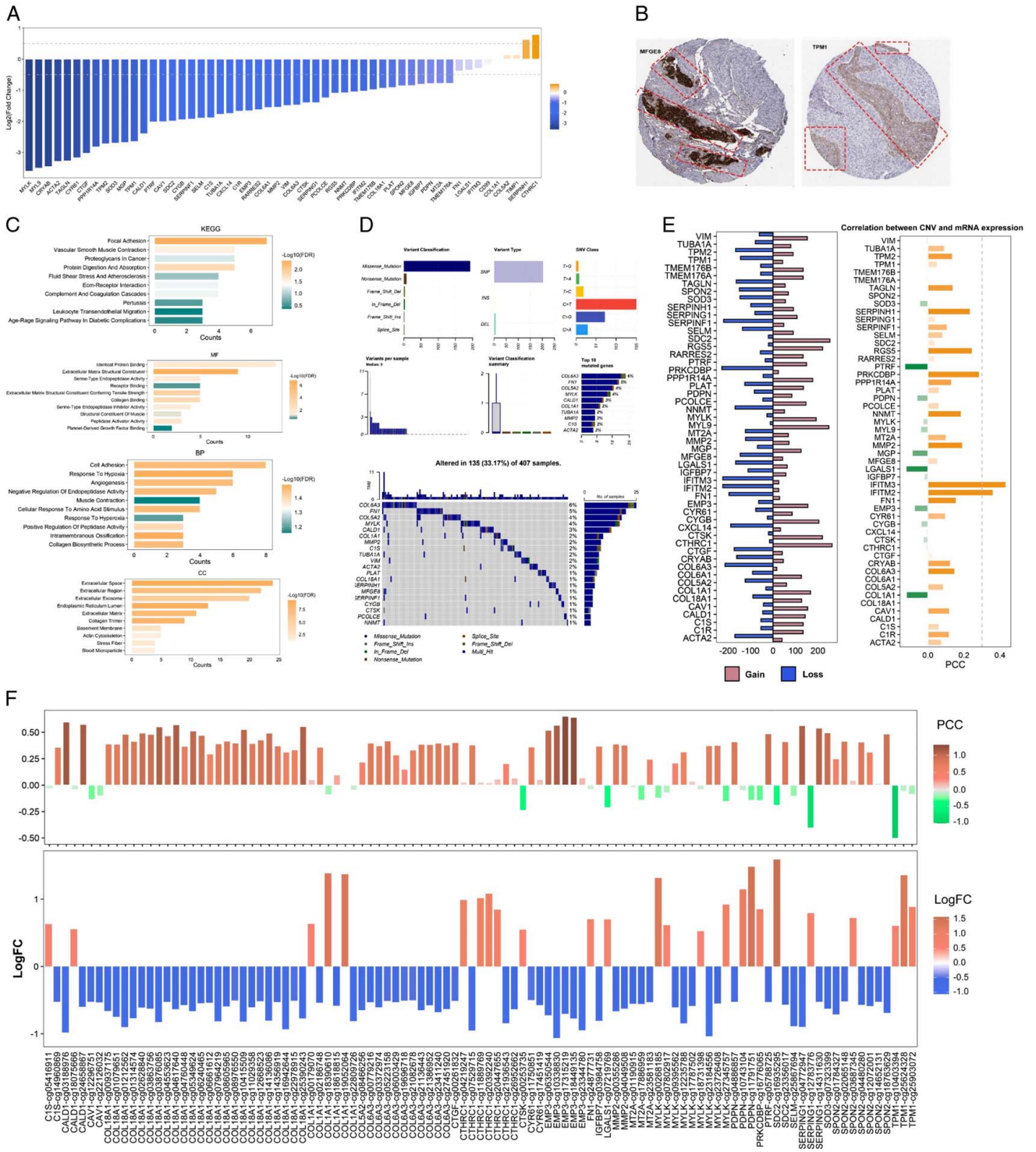

Figure 2. Multiomic analysis of FRG. (A) Barplot represents the logFC per FRG between TCGA-BLCA and adjacent normal tissues. The blue represents the down-regulated FRG, and the orange represents the up-regulated FRG. (B) The immunohistochemistry diagrams show the protein expression distribution of FRG. (C) Barplot shows the KEGG pathway and Gene ontology (GO) enrichment of FRG. (D) Mutation characterisation of FRG in TCGA-BLCA. (E) CNA characterisation of FRG and the correlation between linear copy number and gene mRNA expression. (F) The down barplot shows the logFC of the DNA methylation region representing FRG. The top barplot shows the correlation between DNA methylation levels and mRNA expression per FRG in TCGA-BLCA.

sites are primarily located in body and island regions. However, most sites with upregulation of methylation level show a negative correlation with corresponding gene mRNA expression. The negative correlation sites mainly lie in promoter regions, indicating that methylation alteration on the promoter of these genes silences gene mRNA expression (Fig. 2F and Fig. S4B, Supplemental Digital Content 2, http://links.lww.com/JS9/C616).

Importance evaluation of FRG

We then tried every means to evaluate the importance and clinical relevance of FGRs. We found that 44.4% of them (24/54) were identified as understudied genes (score <100) in terms of their PubTator scores, which, on behalf of the number of publications, correlated to those given genes (Fig. 3A, Table S4, Supplemental Digital Content 4, http://links.lww.com/JS9/C618). Nevertheless, 12.9% of genes with PubTator scores over 1000, especially FN1, showed the highest score, suggesting the most pervasively studied gene that had ever been done. Next, we paid attention to the drug development status of FRG based on the target development levels (TDLs), which were evaluated by the Illuminating the Druggable Genome (IDG) project of NIH. Only 5.6% (3/54) genes are identified to be Tclin (targeted by approved drugs, including CIS, CIR, and PLAT), and 12.96% (7/54) genes to be Tchem (targeted by small molecules that satisfy the activity thresholds, including TUBA1A, NNMT, CRYAB, CTSK, MYLK, MMP2, and FN1). Most genes (79.63%, 43/54) are identified to be Tbio, which do not have known approved drug and small molecule activities. Only one gene has been referred to as Tdark (having very few studies and does not satisfy the criteria of Tchem, Tclin, and Tbio) - SELM. These organised data indicate that there is still a need for more research to prove their function and clinical actionable potential. We further observed the gene dependency score (gDS) of these genes on bladder cancer cells. gDS were used to estimate the importance of a gene by measuring the effect of a given gene deletion on the activity of individual tumour cells[50]. Interestingly, we found in bladder cancer cells, only several genes, such as IFTM3, IFTM2, CTSK, TUBA1A, TPM2, TPM1, and COL1A1 show a lower gDS in most bladder cancer cells, indicating that these genes, especially IFTM3, could affect activities of cells to some extent (Fig. 3B). Most genes show a high gDS in bladder cancer cells, and only several genes show a lower gDS in limited cells. In fact, in ~1000 human cancer cells representing different systems, most FRG only show an essential (i.e. gDS <0) in less than 50% of cells, except for IFITM3, which shows a strict essential (i.e. gDS < – 1) in over 50% cells, no other gene with gDS < – 1 in any cells (Fig. 3C, Fig. S5A and B, Supplemental Digital Content 2, http://links.lww.com/JS9/C616), indicating that high gDS score of FRG in bladder cancer cells is not a peculiar phenomenon, but is a pervasive events in most cancer cells. However, considering their function and location, we could speculate that deletion of these genes might play antitumour roles by inhibiting fibroblasts or other stromal functions. The results of gDS on bladder cancer cells seem to make it quite clear that FRG are not made for targeting tumour cells. We further explore the correlation between FRG and clinical outcomes. In univariate Cox regression analysis, we found most genes show a high risk for bladder cancer patient's overall survival (i.e. HR > 1 and *P*-value <0.05) (Fig. 3D). Even though some genes do not have a relation with prognosis, there is a risk trend for patients' poor outcomes. By applying the surv_cutpoint R-function, the ideal cut-off value for each prognosis-related FRG for prognosis was subsequently determined. Then, the TCGA-BLCA was divided into two groups, high-expression and low-expression groups, based on ideal cut-off value of mRNA expression of individual FRG. We observed that patients with high-expression of these genes showed a worse clinical outcome than those with low-expression of these genes (Fig. 3D and Fig. S6, Supplemental Digital Content 2, http://links.lww.com/JS9/C616). Furthermore, the heatmap revealed that most genes were correlated with stage (94.44% genes, 51/54) and grade (88.89% genes, 48/54) in bladder cancer, appearing that high-expression of these genes accompanied by advanced stage and grade, indicating that these fibroblast-derived genes might promote the progression of cancer (Fig. S5C and D, Supplemental Digital Content 2, http://links.lww.com/JS9/C616). Further validation was carried out across the pan-cancer landscape, and the results showed that over 50% of genes are a risk factor for cancer patients' prognosis in BLCA, KIRC, KIRP, LGG, MESO, STAD, and UVM (Fig. 3E). All in all, these fibroblast-derived genes turn out to be risk factors for bladder cancer patient's prognosis and even patients with other cancer types.

FRG risk signature and nomogram construction

To identify the most relevant genes to the prognosis of patients with bladder cancer, we matched the mRNA expression of FRG and overall survival data. Then, we performed further screening based on ten types of machine learning - Stepwise, Cox boost, Ridge, Enet, Lasso, RSF, plaRcox, GBM, Pamr, and Boruta (Fig. 4A, Table S5, Supplemental Digital Content 5, http://links.lww.com/JS9/C619). After overlapping the genes determined by these methods, three genes were eventually verified - CRYAB, FN1, and COL6A1. Then, three genes were submitted to proceed to multivariate Cox regression analysis. Based on the coefficient and expression per gene, a score called FRG index (FRGI) was finally calculated, that is:

$$\begin{aligned}\mathrm{FRGI} = {} & 0.02982 * \mathrm{Exp}(\mathrm{COL6A1}) \\ & + 0.07886 * \mathrm{Exp}(\mathrm{CRYAB}) \\ & + 0.08066 * \mathrm{Exp}(\mathrm{FN1})\end{aligned}$$

The FRGI was further used to predict prognosis and validated by other bladder cancer and pan-cancer datasets. In four independent BLCA datasets, higher FRGI was usually associated with advanced stage and grade, even though the correlation was not always significant in a single dataset, but the trend turned out to be accordant (Fig. 4B, Fig. S7A-E, Supplemental Digital Content 6, http://links.lww.com/JS9/C620). However, FRGI shows a weak or no correlation between age and sex. Intriguingly, higher FRGI often matches with the worse chemotherapeutic response, indicating tumours with infiltration of fibroblasts that, with FRG expression, could resist chemotherapeutic efficacy (Fig. S7A, Supplemental Digital Content 6, http://links.lww.com/JS9/C620). In addition, high FRGI group patients show a low overall survival probability than low FRGI group, and the number of dead patients in high FRGI group is far more than in low FRGI group in multiple independent BLCA datasets (TCGA-BLCA, GSE13507, GSE31684, IMvigor120, GSE32894, and GSE48276) (Fig. 4C, Fig. S8A, Supplemental Digital Content 6, http://links.lww.com/JS9/C620). Furthermore, patients in the high FRGI group show a higher recurrence risk than those in the low FRGI group (Fig. S8B, Supplemental Digital Content 6,

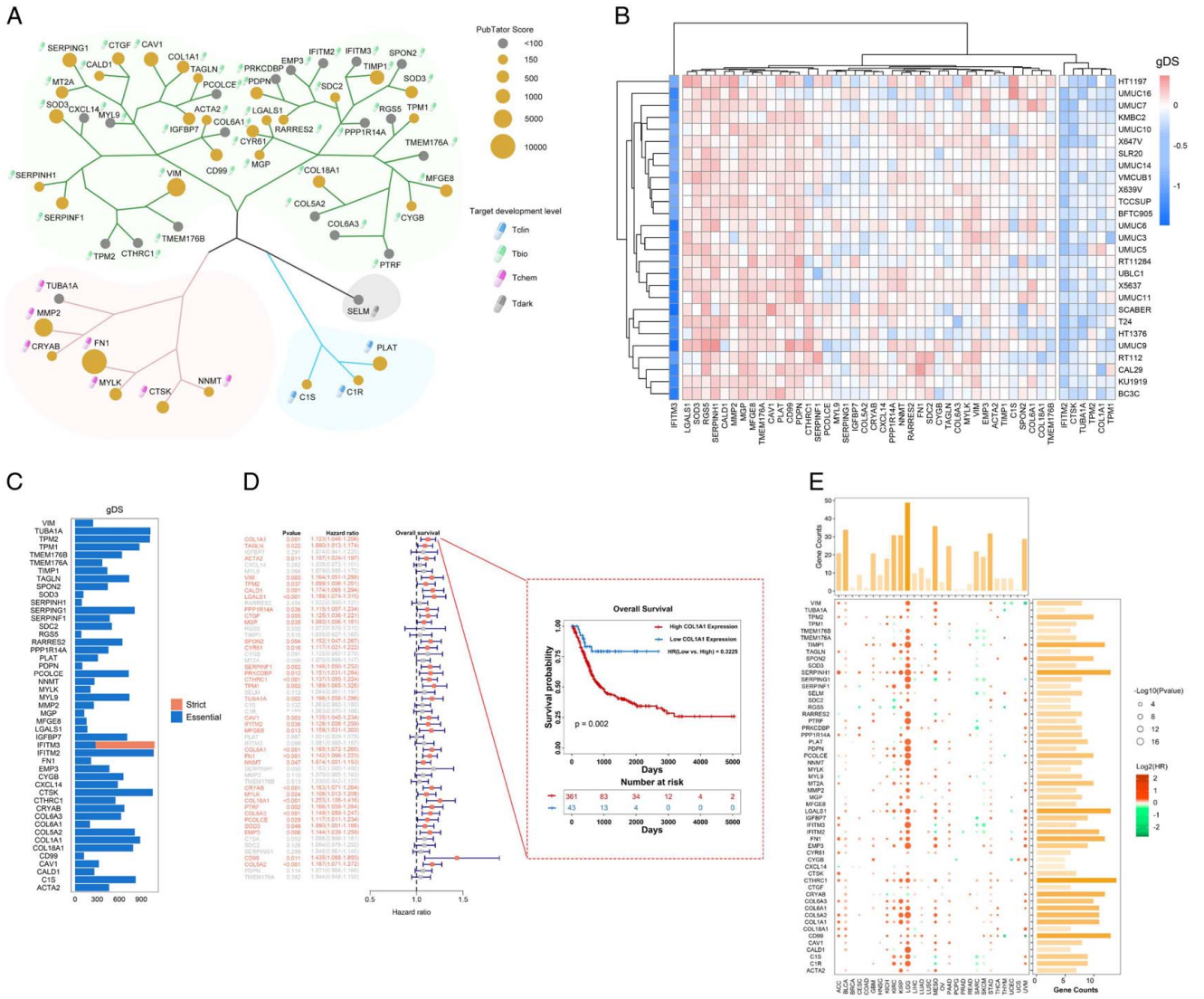

Figure 3. Target development levels (TDLs), gene Dependency Score (gDS), and clinical relevance of FRG. (A) Summary of PubTator scores and TDLs per FRG. The bubble size indicates PubTator scores, and the FRG with a score <100 is shown by a grey bubble. The capsules with different colours represent distinct types of TDLs: blue, Tclin; green, Tbio; purple, Tchem; grey, Tdark. The phylogenetic trees are generated to show all information on PubTator scores and FRG TDLs. (B) The heatmap shows the gDS per FRG in different cells representing bladder cancer. The shade of colour indicates the value of gDS; blue indicates gDS <0, while red indicates gDS > 0. (C) Barplot shows the number of cells across pan-cancer about individual FRG identified with strict (gDS < – 1) or essential (– 1 < gDS <0). (D) The Forest plot shows the relation between identified FRG expression and overall survival in TCGA-BLCA. Based on the prognosis-related gene expression, the sample is divided into high and low-expression groups; the Kaplain–Meier survival curve was depicted to demonstrate the prognostic difference between these two groups. (E) The heatmap shows the hazard ratio (HR) of FRG in terms of overall survival across 28 cancer types. The red bubble indicates FRG with HR > 1 and *P*-value <0.05, and the green bubble shows FRG with HR <0 and *P*-value <0.05. The size of the bubble represents the significance. The barplot shows the number of prognosis-related genes per cancer or the number of cancers from which individual genes were correlated with their prognosis.

http://links.lww.com/JS9/C620). When the patients were divorced by different clinical subgroups (i.e. in terms of age, patients were separated into age > 60 and age ≤ 60 groups), it still seems that high FRGI groups show a worse outcome than low FRGI groups in independent datasets (GSE31684, GSE32894, IMvigor_120, and TCGA-BLCA), indicating FRGI was practical and robust for various clinical subgroups of bladder cancer patients (Fig. S9, Supplemental Digital Content 6, http://links.lww.com/JS9/C620). Then FRGI and other clinical variables were merged to conduct univariate Cox regression analysis, and significant prognostic-related variables were submitted to multivariate Cox regression analysis. The results proved that FRGI was an independent prognostic factor after being adjusted by other clinical variables in the TCGA-BLCA dataset (Fig. 4D). In the GSE32894 datasets, the FRGI shows no significance during the multivariate Cox regression, the higher hazard ratio than other variables showed that FRGI is not able to be ignorant on predicting bladder cancer overall survival (Fig. S10A, Supplemental Digital Content 6, http://links.lww.com/JS9/C620). In the IMvigor_120 dataset, after adjusting by therapy response and metastasis, FRGI showed an independent factor on prognosis (Fig. S10B, Supplemental Digital Content 6, http://links.lww.com/JS9/C620). In addition, we also observed the effect of variables on recurrence-free survival of bladder cancer,

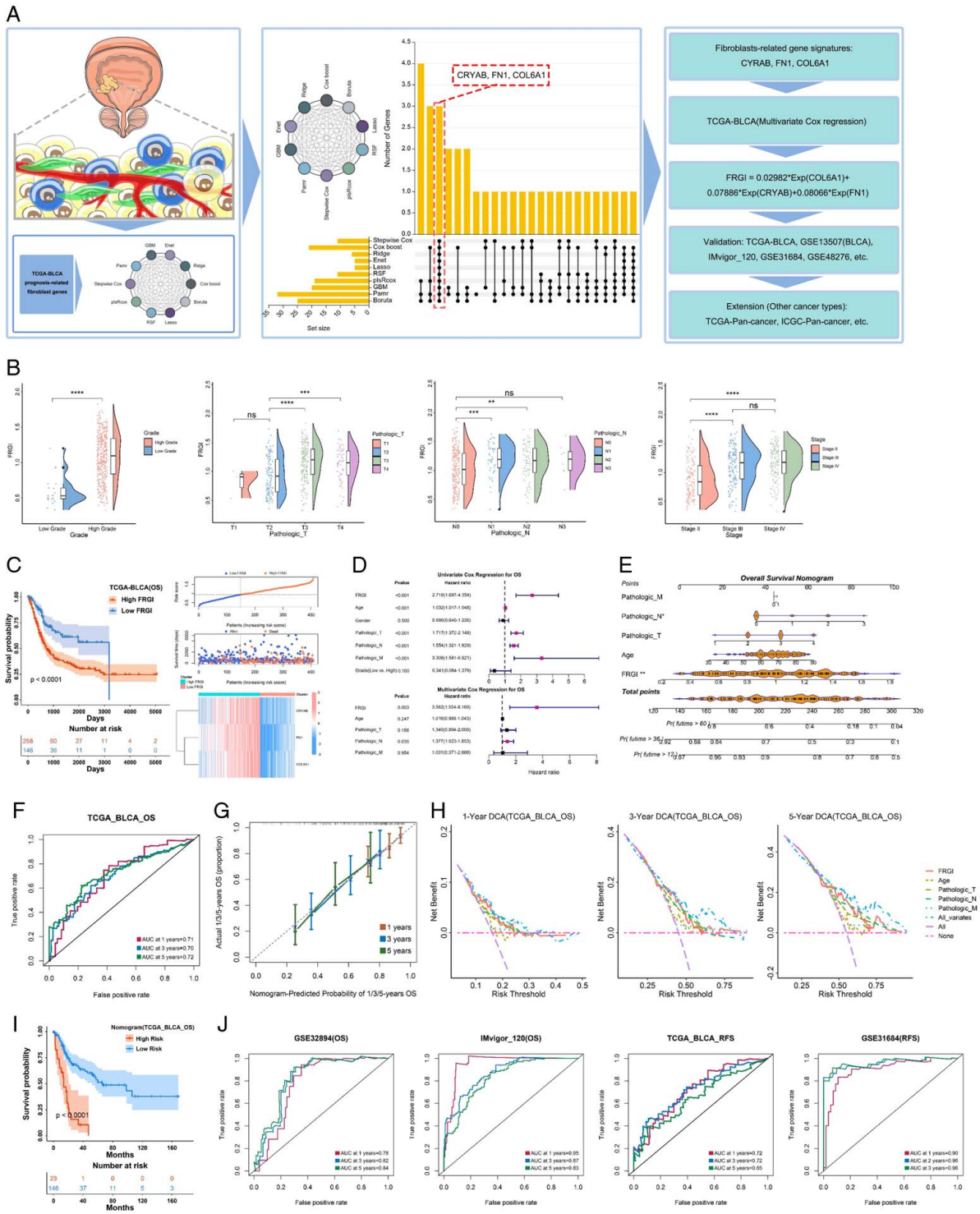

Figure 4. FRG index (FRGI) and nomogram model construction. (A) The flow chart shows the expression profile of FRG in TCGA-BLCA was submitted to conduct machine learning, and the three overlapping genes were determined to construct FRGI; then, the FRGI was validated by various datasets representing bladder cancer and other cancer types. (B) The diagrams show the FRGI alteration in different grades, pathologic_ T, pathologic_N, and pathologic stage. (C) The survival curve, risk dot-plot, and heatmap show the OS rate, distribution of alive and dead patients, and FRG expression in high/low FRGI groups. (D) The forest plot shows the univariate and multivariate Cox regression results of FRGI and other clinical variables to prognosis in the TCGA-BLCA dataset. (E) A nomogram was constructed from the variables of multivariate Cox regression to predict the 3-/5-/7-year survival probability. (F–H) Time-dependent ROC curve, calibration curve, and decision curve analysis (DCA) of nomogram model on predicting TCGA-BLCA OS. (I) The Kaplain–Meier survival curve shows the survival probability of high and low-risk groups based on the nomogram model. (J) Time-dependent ROC curve of nomogram on bladder cancer OS or RFS from other datasets (including GSE32894, IMvigor_120, TCGA-BLCA, and GSE31684). *P-value <0.05; **P-value <0.01; ***P-value <0.001; ****P-value <0.0001; NS, no significance.

the result revealed that FRGI has a risk effect on recurrence-free survival in univariate Cox regression analysis but not as an independent risk factor during multivariate Cox regression analysis (Fig. S11A and B, Supplemental Digital Content 6, http://links.lww.com/JS9/C620). We further constructed the nomogram using the variables in multivariate Cox regression analysis to predict the 1-/3-/5-year survival rate of bladder cancer (Fig. 4E). Time-dependent ROC curve and calibration curve revealed that the nomogram showed high accuracy in predicting the prognosis (For TCGA-BLCA OS: AUC at 1 year = 0.71, AUC at 3 years = 0.70, AUC at 1 year = 0.72; For GSE32894 OS: AUC at 1 year = 0.78, AUC at 3 years = 0.82, AUC at 1 year = 0.84; For IMvigor_120 OS: AUC at 1 year = 0.95, AUC at 3 years = 0.87, AUC at 1 year = 0.83; For TCGA-BLCA RFS: AUC at 1 year = 0.72, AUC at 3 years = 0.72, AUC at 1 year = 0.65; For GSE31684 RFS: AUC at 1 year = 0.90, AUC at 3 years = 0.96, AUC at 1 year = 0.96). Decision curve analysis revealed the highest clinical benefit when selecting all variables compared to each single one. In addition, the risk score constructed by nomogram model showed the most discriminate difference of survival probability in high-/low-risk groups (Fig. 4F-J, Fig. S10A and B, Supplemental Digital Content 6, http://links.lww.com/JS9/C620, Fig. S11A and B, Supplemental Digital Content 6, http://links.lww.com/JS9/C620). We further validate the FRGI in other cancer types, and the result bears a resemblance to bladder cancer. That is, the high FRGI showed a worse outcome than the low FRGI (Fig. S12A and B, Supplemental Digital Content 6, http://links.lww.com/JS9/C620). These results revealed that FRGI could not only predict the survival probability of bladder cancer but also extend to other cancer types.

Fibroblasts subtype determination

Based on the significance of FRGI on the prognosis of bladder cancer, we generated the fibroblast subtype by calculating Euclidean distance among samples based on FRG signature expression. Fibroblast hot type (the high-expression on FRG signature) and cold type (the low-expression on FRG signature) were generated (Fig. 5A). Fibroblasts subtype was correlated with tumour progression, showing that advanced tumour stage and grade are primarily located in fibroblasts hot type, and the fibroblasts hot type shows a worse outcome than the fibroblasts cold type (Fig. 5B). These results were further validated in four extra independent cohorts (Fig. S13A-D, Supplemental Digital Content 6, http://links.lww.com/JS9/C620). We replaced the FRGI with the fibroblast subtype to conduct subsequent mechanism analysis. The wide-genome mRNA expression profile of bladder cancer ordered by fibroblast subtype was submitted to gene set enrichment analysis (GSEA) software. Then, the distinct enrichment pathways were identified based on the hallmark cancer pathways (Fig. 5C). The results represented that multiple cancer-related pathways were highly enriched in fibroblast hot type, and the top 20 pathways in five dependent datasets were shown (Fig. 5D). Among these, several pathways showed universally high enrichment in fibroblast hot type, mainly including TNFA signalling VIA NFKB, KRAS signalling UP, INTERFERON GAMMA RESPONSE, INFLAMMATORY RESPONSE, IL6 JAK STAT3 signalling, IL2 STAT5 signalling, HEDGEHOG signalling, EPITHELIAL MESENCHYMAL TRANSITION, COMPLEMENT, etc. (Fig. 5E, Table S6, Supplemental Digital Content 7, http://links.lww.com/JS9/C621). To further validate, we calculated the activity score of 50 hallmark pathways, and the correlation between hallmark pathways and FRGI was further calculated according to the Pearson method (Fig. 5F). As we expected, FRGI showed a highly positive correlation with the pathways mentioned above in five BLCA datasets (Fig. 5G, Table S7, Supplemental Digital Content 8, http://links.lww.com/JS9/C622), indicating that these fibroblast-derived genes might activate these pathways to promote tumour prognosis or malignant phenotype. In addition, we found FRGI negatively correlated with several pathways, such as OXIDATIVE_PHOSPHORYLATION and PEROXISOME pathways. All in all, these pathway alterations might be potential reasons for the poor prognosis of cancer patients. We further contrast several phenotypes that are associated with bladder cancer. Our previous study revealed that primary cilium deletion causes malignant behaviour in bladder cancer cells and promotes SHH pathways. In this study, we also find several PC-degradation-related genes showed a higher expression in fibroblast hot type, revealing that fibroblast infringement on tumour might correlate with PC degradation (Fig. S14A, Supplemental Digital Content 6, http://links.lww.com/JS9/C620). When bladder cancer was separated into different molecular subtypes, we found a large proportion of basal type located in fibroblast hot type, P53-like subtype, and stroma-rich type (Fig. S14B, Supplemental Digital Content 6, http://links.lww.com/JS9/C620, Table S8, Supplemental Digital Content 9, http://links.lww.com/JS9/C623). Furthermore, bladder cancer immune subtype C2 is mainly situated in the fibroblast hot type, while C1 and C4 lie in the fibroblast cold type (Fig. S14C, Supplemental Digital Content 6, http://links.lww.com/JS9/C620).

Fibroblast type associate with immune therapeutic response

Accumulating evidence revealed that fibroblast could mediate immune cell activity and suppress antitumour immune response. As shown in Figure 1F, these fibroblast-derived genes showed a weak or negative correlation with immune-related cells, which triggers us to investigate further whether fibroblasts affect immune therapeutic efficacy. Thus, we utilised tumour immune dysfunction and exclusion (TIDE), a public website integrated with large-scale omics data and biomarkers based on immune-checkpoint blockade (ICB) trials[51], to predict the potential patients who were sensitive to immune therapy or not. In accordance with the TIDE score, the responder and nonresponder of bladder cancer patients were recognised in TCGA-BLCA (Fig. 6A). As expected, nonresponders showed a worse outcome than responders, indicating that immune system activation could prolong patients' survival rate. In addition, we found that non-responders were mainly distributed in the high FRGI group or fibroblast hot type (P-value <0.0001, χ^2 test), suggesting that fibroblast enrichment could inhibit immune therapeutic effect (Fig. 6A and Fig. S15A, Supplemental Digital Content 10, http://links.lww.com/JS9/C624). The area under the curve (AUC) based on ROC revealed that the accuracy of FRGI predicting immune therapeutic response is 0.8642, and nonresponders show a higher FRGI. We further conducted the same analysis in three other independent bladder cancer datasets (GSE31684, GSE13507, and GSE32894), and the results bear a resemblance to TCGA-BLCA (Fig. 6B-D, Fig. S15A, Supplemental Digital Content 10, http://links.lww.com/JS9/C624). In the metastatic immune therapeutic cohort, we also observed patients with stable disease and

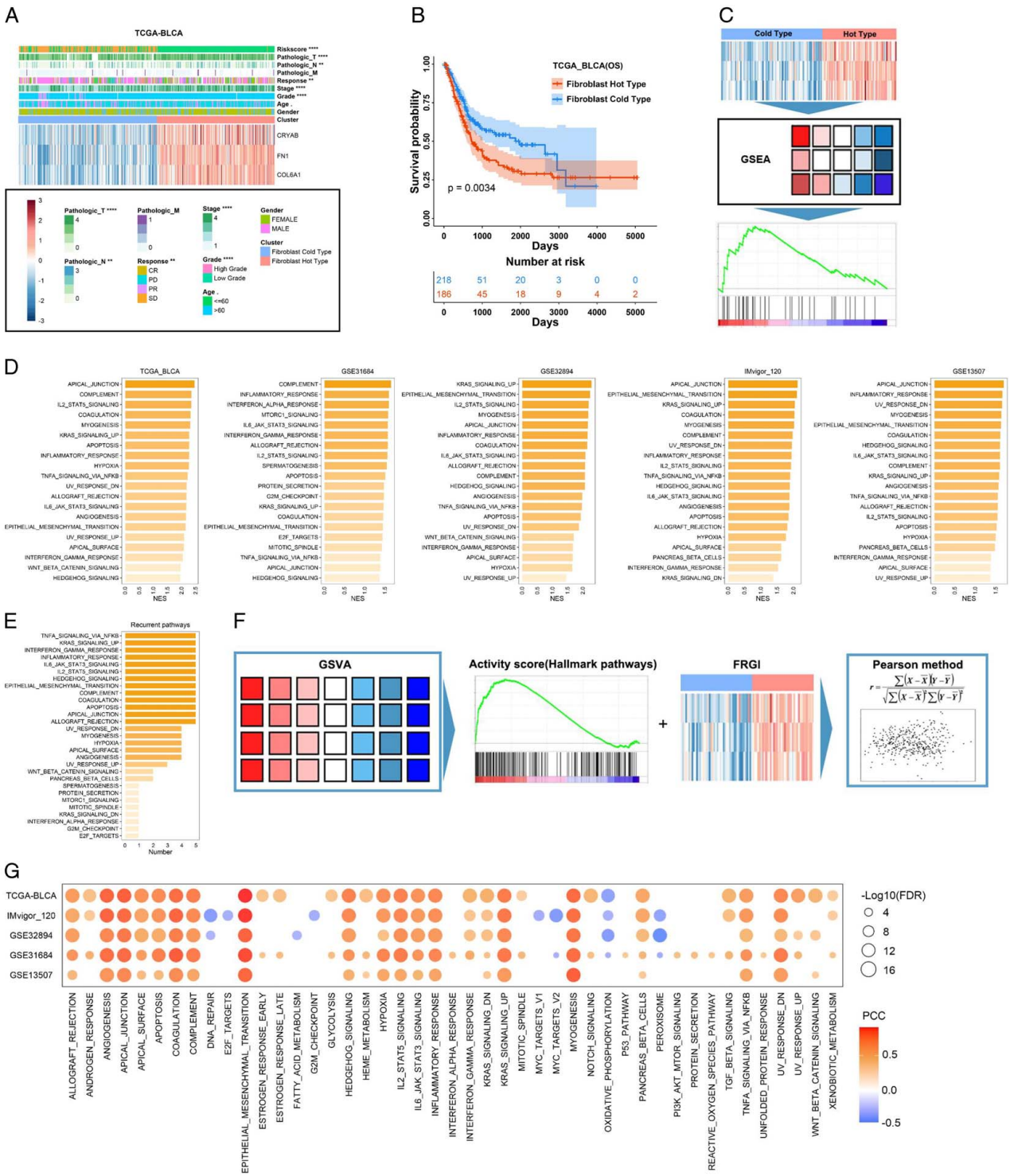

Figure 5. FRG subtype and mechanism. (A) Distribution of FRG expression and clinical variables (including FGI, pathologic_T, pathologic_N, pathologic_M, response, stage, grade, age, and gender) in FRG hot and cold type. (B) Kaplain–Meier survival curve shows the survival difference between FRG hot and cold types. (C) The flow chart reveals the progression of mechanism excavation: normalised mRNA expression data ordered by the FRG subtypes was submitted to GSEA software to evaluate the differentially enriched pathways. (D) Barplot shows the top 20 highly enriched pathways in FRG hot type in TCGA-BLCA, GSE31684, GSE32894, GSE13507, and IMvigor_120 datasets. (E) Barplot shows the recurrent enrichment pathways in FRG hot type across five datasets. (F) Flow chart reveals the GSVA analysis progression: normalised data was submitted to GSVA to calculate the activity score of cancer-related hallmark pathways; then, the Pearson method was utilised to compute the Pearson correlation coefficient (PCC) between FRGI and the activity score of pathways. (G) The heatmap reveals a correlation between FRGI and the activity score of hallmark pathways. The size of the bubble reveals the significance, and the shade of colour reveals the PCC, red represents PCC >0. blue represents PCC <0. *P-value <0.05; **P-value <0.01; ***P-value <0.001; ****P-value <0.0001; NS, no significant.

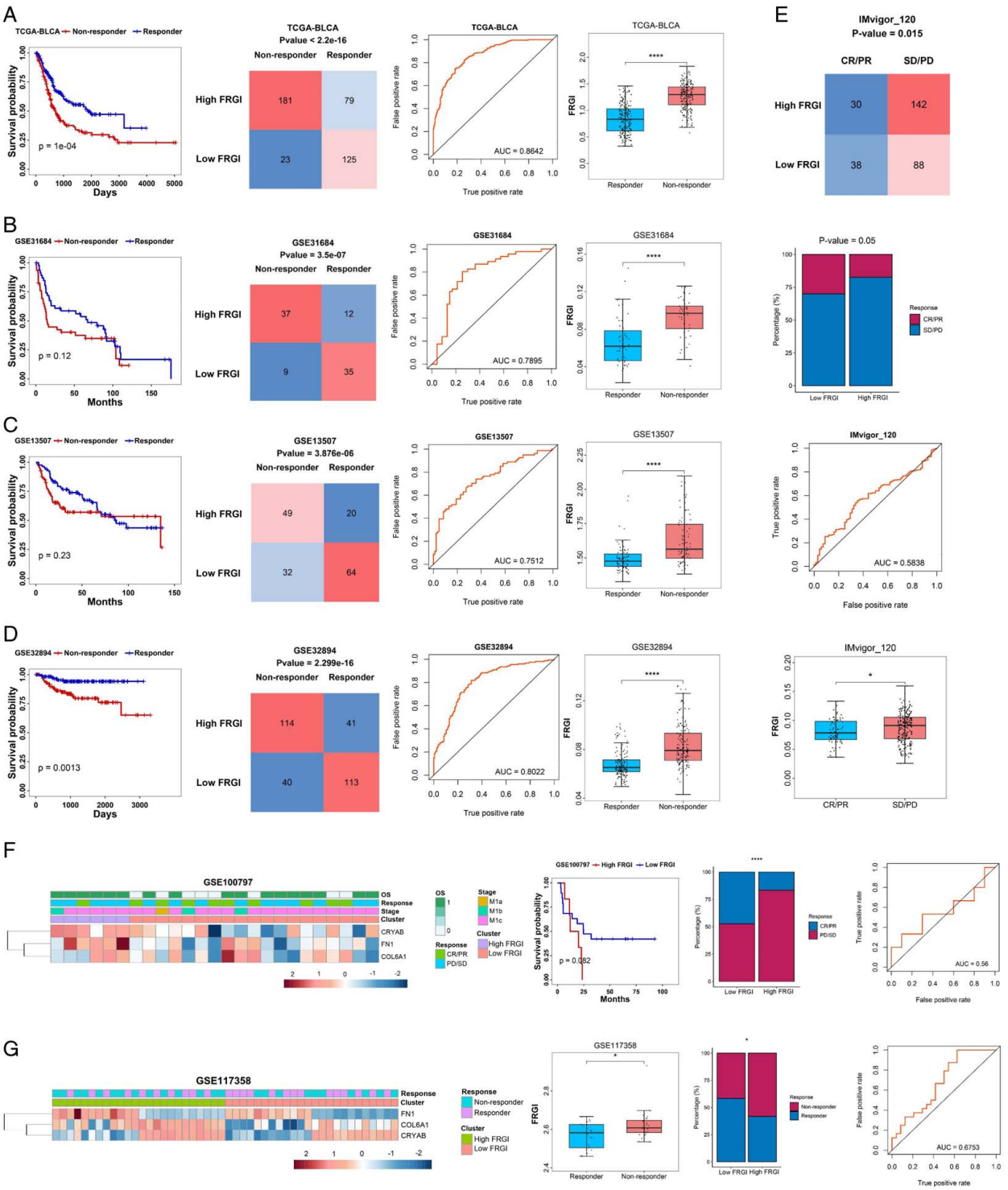

Figure 6. FRGI and FRG subtypes predict immune therapeutic response. (A–E) Kaplain–Meier survival curve reveals the overall survival difference between responders and nonresponders determined by the TIDE score in datasets. Block charts or histograms show the distribution of responders and nonresponders in high FRGI and low FRGI groups. ROC curves show the predicted capacity of FRGI on immune therapeutic response. Boxplot shows the FRGI difference between responders and nonresponders. (F) Heatmap reveals the correlation between the FRGI group and FRG expression, OS, stage, and therapeutic response in the GSE100797 dataset. Kaplain–Meier survival curve reveals the overall survival difference between high FRGI and low FRGI groups, and the histogram shows the distribution of therapeutic response in high or low FRGI groups. ROC reveals the predicted capacity of FRGI on immune therapeutic response. (G) Heatmap reveals the correlation between the FRGI group, FRG expression, and therapeutic response in the GSE117358 dataset. Boxplot reveals the FRGI difference in responder and non-responder groups. The histogram shows the distribution of therapeutic response in high or low FRGI groups. ROC reveals the predicted capacity of FRGI on immune therapeutic response. **P*-value <0.05; ***P*-value <0.01; ****P*-value <0.001; *****P*-value <0.0001; NS, no significant.

progression disease stand in higher proportion in the high FRGI group than in the low FRGI group (Fig. 6E). Even though the AUC was low (0.5838), the FRGI was still higher in SD/PD group than in CR/PR group. We generate the FRGI in other cohorts representing melanoma, nonsmall cell lung carcinoma, and glioblastoma; the results also show the outcome of the high FRGI group was poorer than that of the low FRGI group (Fig. S15B-E, Supplemental Digital Content 10, http://links.lww.com/JS9/C624, Fig. S15G, Supplemental Digital Content 10, http://links.lww.com/JS9/C624). In the immune therapeutic cohorts representing melanoma, the high FRGI group shows a worse prognosis and poor response to immune therapy (for GSE100797, AUC = 0.56; for GSE19293, AUC = 0.5908) (Fig. 6F, Fig. S15F, Supplemental Digital Content 10, http://links.lww.com/JS9/C624). Intriguingly, in the mice cohort with mesothelioma and kidney cancer, nonresponder shows a higher FRGI, a higher proportion of nonresponders located in the high FRGI group, and the AUC for FRGI to predict therapeutic response is 0.6753 (Fig. 6G). All in all, these results revealed that the fibroblast subtype or FRGI could not only predict the immune therapeutic response in bladder cancer but also evaluate the effect of other cancers to some extent.

CD8 + T-cells - fibroblast subtype construction, mechanism, epigenetic alteration

We further explore the association of FRGI and the immune system in bladder cancer. Through analysing the correlation between FRGI and 75 immune-related genes[52], we found FRGI is positively correlated with most immune-related genes across five bladder cancer datasets, including several immunosuppressive molecules, such as PDL1 (PDCD1), PDL2 (PDCD1LG2), CD80, EDNRB, MICA, and MICB. Interestingly, FRGI showed a highly positive correlation with VEGFB but a negative correlation with VEGFA; these two genes were reported to play the role of immune suppressor (Fig. S16A, Supplemental Digital Content 10, http://links.lww.com/JS9/C624). In addition, the fibroblast hot type shows a higher immune score, stromal score, and microenvironment score (Fig. S16B, Supplemental Digital Content 10, http://links.lww.com/JS9/C624). For the fraction of immune cells, we observed that B cell memory shows no significant alteration or slight decrease in fibroblast hot types (Fig. S16C, Supplemental Digital Content 10, http://links.lww.com/JS9/C624). The fraction of CD8 T-cells does not alter between these two subtypes across five datasets, while NK cells activated also show no change in most datasets except GSE32894. Tregs fraction shows a slight increase in IMvigor_120 but a decrease or no alteration in other datasets. All in all, the fraction of immune cells across these five datasets fluctuates severely. We further explored the relation between immune cell activity score and FRGI or fibroblast subtype. Whatever fibroblast subtype and FRGI, we found immunosuppressive cells-Tregs and M2 macrophage highly activated in fibroblast hot type and high FRGI group in five bladder cancer datasets (Fig. 7A and B, Fig. S17A and B, Supplemental Digital Content 10, http://links.lww.com/JS9/C624). However, the activity of antitumour immune cells - CD4 + T-cells, CD8 + T-cells and NKT, showed no significant difference in fibroblast subtypes and high-/low-FRGI groups. FRGI showed a positive correlation with Tregs, M1, and M2 macrophage activity but no correlation or negative correlation with CD4 + T-cells, CD8 + T-Cells, and NKT (Fig. 7C and Fig. S17C, Supplemental Digital Content 10, http://links.lww.com/JS9/C624). It seems to indicate that fibroblasts could activate the Tregs and M2 macrophage to inhibit the immune system. However, as it is said that antitumour immune response is associated with not only one factor, considering that antitumour immune cells are largely associated with immune therapeutic effect, utilising a single FRG signature to estimate whether a patient with a tumour is sensitive or resistant to immune therapy is apparently one-sided[53]. Therefore, we tried to combine FRG signature and antitumour immunity to proceed with further research. In five independent bladder cancer datasets, we conducted survival analysis based on the activities of three antitumour immune cells - CD4 + T-cells, CD8 + T-cells, and NKT. We found CD8 + T-cells bear a resemblance to the result in each dataset; that is, high CD8 + T-cell activity shows a better prognosis than low activity, while the other two cells were not stable in five datasets (Fig. S18A, Supplemental Digital Content 10, http://links.lww.com/JS9/C624), representing that CD8 + T-cells were eligible to bind with fibroblast to construct a new stable subtype. It has been reported that tumours with growing infiltration of CD4 and CD8 T-cells turn out to be immune-inflammatory tumours, also called hot tumours, which are referred to as immunoreactive[54]. However, CD8 + T-cells are well enough to be a signal to classify as immunologically cold and hot tumours[55]. These results support us in combining CD8 + T-cells and our constructed FRG signature. By ideal cut-off value, high-/low-CD8 + T-cells activity was determined and combined with fibroblast subtype, and a CD8 + T-cells -fibroblast subtype was subsequently constructed, including high CD8 + T-cells activity fibroblast hot type (CD8 + FH), high CD8 + T-cells activity fibroblast cold type (CD8 + FC), low CD8 + T-cells activity fibroblast hot type (CD8-FH), low CD8 + T-cells activity fibroblast cold type (CD8-FC). Patients in the CD8 + FC type show the best prognosis, and those in the CD8-FH type represent the worst prognosis in TCGA-BLCA datasets (Fig. 7D). Moreover, the same results were observed in GSE31684, IMvigor_120, and GSE32894, except for GSE13507 datasets (Fig. S17D, Supplemental Digital Content 10, http://links.lww.com/JS9/C624). Interestingly, in the same CD8 + T-cells activity group, the fibroblast hot type always shows a worse prognosis. In other datasets representing different cancer types, we also observed similar results (Fig. S18B, Supplemental Digital Content 10, http://links.lww.com/JS9/C624). In addition, when we predicted the immune therapeutic response using FRGI and CD8 + T-Cells activity, we found the accuracy significantly increased compared to using FRGI single (Fig. S19A, Supplemental Digital Content 10, http://links.lww.com/JS9/C624). We found most patients with CD8 + FC type trend in response to immune therapy, while only a small collection of patients with CD8-FH are sensitive to immune therapeutic response (Fig. S19B and C, Supplemental Digital Content 10, http://links.lww.com/JS9/C624). Another immune therapeutic dataset further validates this point, that is, patients in the CD8 + FC group appear to have more per cent of complete response and partial response (Fig. S19D, Supplemental Digital Content 10, http://links.lww.com/JS9/C624). We further used the GSE91061 dataset, which contains 58 on-treatment (during ICB therapy) and 51 pretreatment (before ICB therapy) melanoma and NSCLC RNA-sequence data, to analyse the dynamic progression of subtype migration. We found that patients with low FRGI and high CD8 + T-cell activity show the highest rate of response in on-treatment data (Fig. S19E,

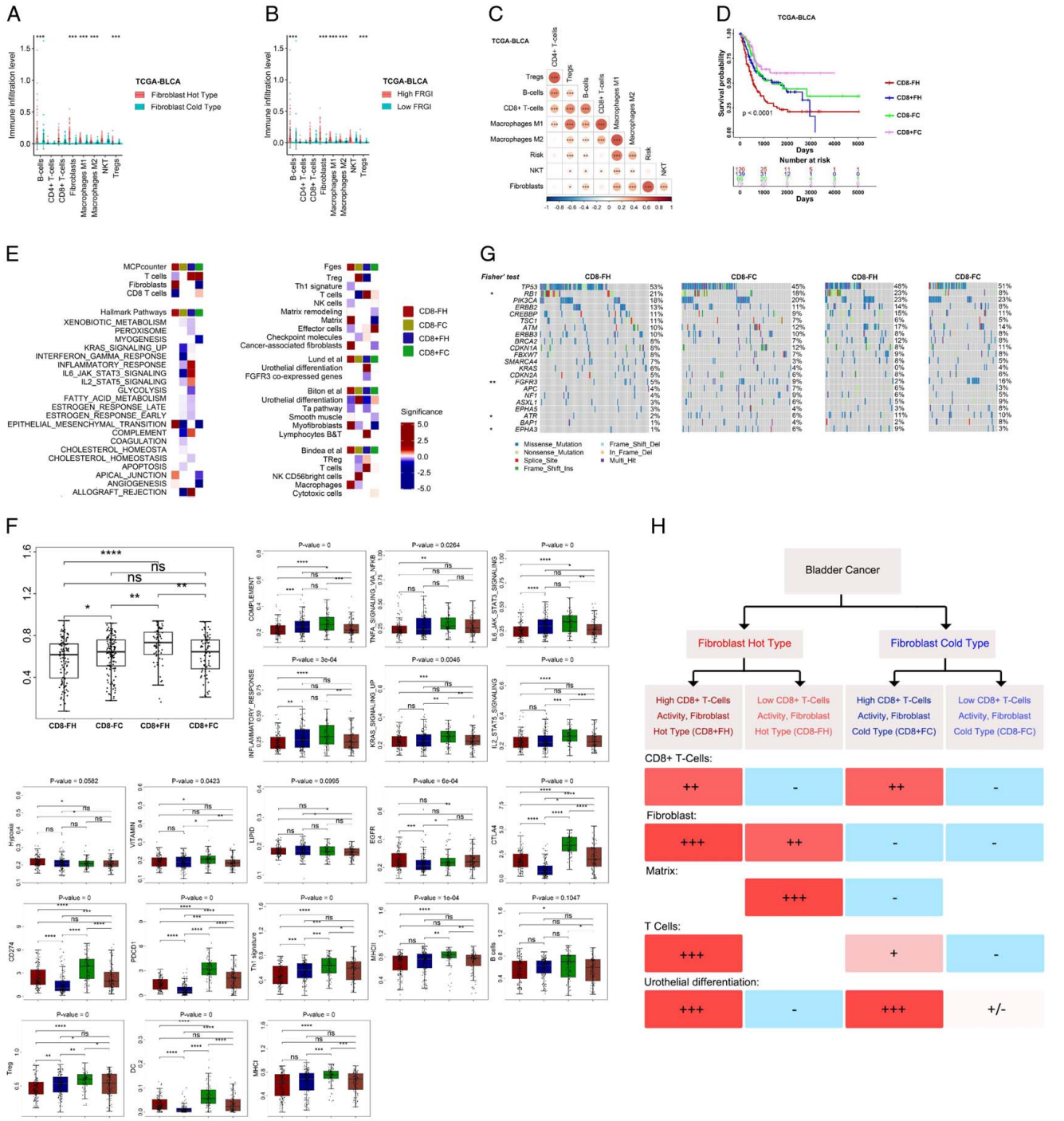

Figure 7. CD8 + T-cells - FRG type construction on predicting prognosis and immune therapeutic response. (A and B) The dot plot shows the activity differences of antitumour immune cells (B-cells, CD4 + T-cells, CD8 + T-cells, NKT, and Macrophage M1) and protumour immune cells (Tregs and Macrophage M2) in high/low FRGI groups and FRG hot/cold subtype in TCGA-BLCA dataset. (C) The heatmap shows the correlation between FRGI and other antitumour/protumour immune cells; red represents a positive correlation, blue represents a negative correlation, and the shade of colour and size of the bubble represent significance. (D) Kaplain–Meier survival curve reveals the survival probability of CD8 + FH, CD8 + FC, CD8-FH, and CD8-FC subtypes in TCGA-BLCA datasets. (E) The heatmap reveals the significant-enriched pathways in four subtypes; the shade of the colour represents significance; red represents high enrichment, and blue represents low enrichment. (F) Boxplot shows the difference of the existing gene signature activity scores in four subtypes. (G) The waterfall plot shows the mutation characterisation of clinically actionable genes across four subtypes. The distribution significance of mutation rate across types was calculated using Fisher's test. (H) Schematic description of the features associated with the four CD8 + T-cells - FRG subtypes. **P*-value <0.05; ***P*-value <0.01; ****P*-value <0.001; *****P*-value <0.0001; NS, no significance.

Supplemental Digital Content 10, http://links.lww.com/JS9/C624). What is more, after matching the on-treatment and pretreatment data of the same patients, we found CD8 + Low FRGI, CD8 + High FRGI, and CD8-High FRGI groups show no migration to other types. However, a small proportion of patients in CD8-Low FRGI group migrate to the CD8 + High FRGI and CD8 + Low FRGI group in the CR/PR cohort. In the SD/PD cohort, patients in CD8-High FRGI group in pretreatment migrate to other types except the CD8 + Low FRGI group. Patients in theCD8 + Low FRGI group could migrate to the other three types with malignant phenotypes (i.e. high FRGI, low CD8 + T-cell activity, or both of them), suggesting that the SD/PD cohort occurred to complex dynamic migration progression, and FRGI combine CD8 + T-cells could depict the migration and explain the reason causes immunotherapeutic insensitivity (Fig. S19E, Supplemental Digital Content 10, http://links.lww.com/JS9/C624). We further analysed the potential mechanism of these four types based on gene set analysis (GSA) and identified gene signatures, different gene signatures highly or lowly enriched in distinct types in the TCGA-BLCA dataset; other three datasets were conducted for further validation (Fig. 7E, Fig. S20A, Supplemental Digital Content 10, http://links.lww.com/JS9/C624). T-cells, for instance, were significantly enriched in CD8 + FC and CD8 + FH types; the EMT pathway was highly enriched in CD8-FH type, JAK_STAT3, and IL2_STAT5 signalling pathways, mainly enriched in CD8 + FH type. Other signatures representing cancer-related pathways, immune checkpoint, and antigen presentation system were further analysed and revealed distinct activity or expression across four types (Fig. 7F). We then used TCGA exome data to identify class-specific mutation and copy number aberrations (CNAs) (Fig. 7G, Fig. S20B and C, Supplemental Digital Content 10, http://links.lww.com/JS9/C624). The genes with mutation rate > 10% across four types were concentrated on. TP53, MUC16, and KDM6A showed a universally high mutation rate (all > 10%) across four subtypes, especially in the CD8 + FC type (Fig. S20B, Supplemental Digital Content 10, http://links.lww.com/JS9/C624). RB1 mutation is mainly enriched in three subtypes except for the CD8 + FC type. CD8 + FH type harboured more frequent mutations of KMT2A and AHNAK, while CD8 + FC type was characterised by enrichment of mutations in DST (20%) and LRP1B (20%). For other clinically actionable genes, FGFR3 (16%) mutation is primarily enriched in the CD8 + FC type (Fig. 7G). ATR shows a higher mutation rate (11 and 10%, respectively) in CD8 + FH and CD8 + FC types. EPHA3 showed the highest mutation frequency in the CD8 + FH type. For copy number, aberrations across types were determined by GISTIC 2.0 software. CD8-FC type was enriched in amplication of CCND1, DDR2, MCL1, NOTCH2,EGFR, MYC, CDH1, VHL, CCNE1, XPO1, etc. CD8-FC type was enriched in the amplification of CCND1, MCL1, ERBB2, CCNE1, FGFR3, etc. In CD8 + FH type, which was enriched in amplification of DDR2, EGFR, CCND1, CCND3, CCNE1, FLT3, ASXL1, etc. While in CD8 + FC type, which was harboured amplication of CCND1, MCL1, FGFR3, CCNE1, MYC, MDM2, ERBB2, AKT3, and so on. These CNAs across subtypes provided the potential to develop targeted drugs based on specific types (Fig. S20C, Supplemental Digital Content 10, http://links.lww.com/JS9/C624, Table S9, Supplemental Digital Content 11, http://links.lww.com/JS9/C625). All in all, we constructed four subtypes based on three fibroblast-derived genes and CD8 + T-cell activity to predict prognosis and immune therapy response in bladder cancer (Fig. 7H). We merged all the information of each type based on multi-omic character and generated a potential therapeutic map, which might provide a basic combined therapy strategy based on subtypes of bladder cancer (Fig. 8).

Methods

Data collection

The work has been reported in line with the REMARK criteria[56] (Supplemental Digital Content 12, http://links.lww.com/JS9/C626). This study did not generate any new data. All data are available on the public website. The scRNA-seq datasets with both malignant and stromal or immune cells data (including GSE135337, GSE130001, GSE165399, GSE166635, GSE173950, GSE166555, GSE138709, GSE148673, GSE123813, GSE167297, GSE111360, GSE151214, GSE115978, GSE103322) representing different type of cancers were obtained from the Gene Expression Omnibus (GEO) (https://www.ncbi.nlm.nih.gov/geo/) and tumour Immune Single-cell Hub 2 (TISCH2) (http://tisch.comp-genomics.org/) (Table S1, Supplemental Digital Content 13, http://links.lww.com/JS9/C627). These datasets cover bladder cancer (BLCA), basal cell carcinoma (BCC), breast cancer (BRCA), colorectal cancer (CRC), cholangiocarcinoma (CHOL), head and neck cancer (HNSC), liver hepatocellular carcinoma (LIHC), ovarian serous cystadenocarcinoma (OV), pancreatic adenocarcinoma (PAAD), skin cutaneous melanoma (SKCM), stomach adenocarcinoma (STAD), oesophageal carcinoma (ESCA), and kidney renal clear cell carcinoma (KIRC). The pan-cancer data, including GSE2109 and TCGA Pan-cancer datasets, were downloaded from the GEO and UCSC Xena (https://xena.ucsc.edu/) websites. TCGA-BLCA dataset acquired from UCSC Xena was utilised to construct the model, and other bladder cancer datasets - GSE13507, GSE31684, GSE32894, and GSE48279 obtained from GEO were used for further validation. In addition, other TCGA datasets across cancer types, including adrenocortical carcinoma (ACC), cervical squamous cell carcinoma and endocervical adenocarcinoma (CESC), colon adenocarcinoma (COAD), oesophageal carcinoma (ESCA), glioblastoma multiforme (GBM), uterine corpus endometrial carcinoma (UCEC), lung squamous cell carcinoma (LUSC), OV, HNSC, brain lower grade glioma (LGG), PAAD, pheochromocytoma and paraganglioma (PCPG), thyroid carcinoma (THCA), rectum adenocarcinoma (READ), kidney chromophobe (KICH), LIHC, KIRC, kidney renal papillary cell carcinoma (KIRP), mesothelioma (MESO), STAD, uveal melanoma (UVM) from UCSC Xena database; PACA-CA, OV-AU, ORCA-IN, CLLE-ES, BPLL-FR, and PANE-AU from ICGC database (https://dcc.icgc.org/); GSE65904, GSE22153, GSE19234, GSE135222 from GEO database were downloaded to further model validation. In addition, immune-related datasets, including IMvigor_120, GSE19293, GSE148467, GSE100797, GSE117358, and GSE91061, were further collected from previous research[57] and GEO datasets, respectively, to predict immune therapeutic response.

For gene sets signature, Fges[47], the microenvironment cell populations-counter (MCP-counter) deconvolution algorithm[49], and immune gene sets[58] were collected from published literature. xCell signature comes from xCell R-package. Cancer-associated hallmark pathways gene signatures were downloaded from the Molecular Signatures Database (https://www.gsea-msigdb.org/gsea/msigdb/index.jsp). Other cell-specific signalling pathways were using PROGENy algorithm (Pathway RespOnsive

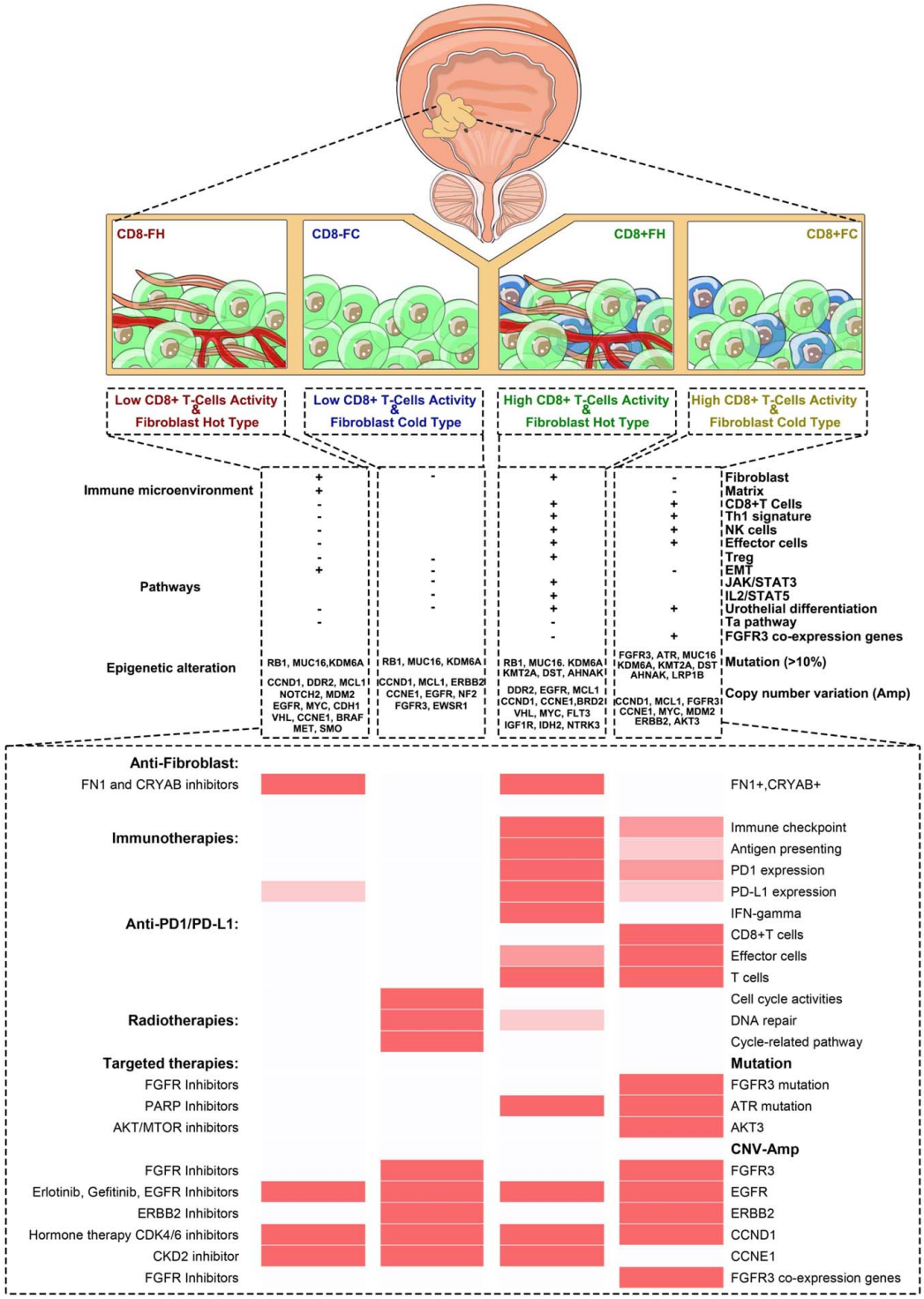

Figure 8. Schematic description of the features associated with the four CD8 + T-cells - FRG subtypes by merging immune microenvironment signature, pathways signature, and epigenetic characterisation, as well as primitive potential comprehensive therapy strategies.

GENes)[59]. Bladder-related gene signatures were obtained from summarised sets of previous research[8].

scRNA-Seq data analysis

We submitted the scRNA-seq dataset GSE135337 to the Seurat R-package. The cells were filtered through the thresholds that: 1) count of detected genes > 50 per cell; 2) the mitochondrial genes percentage <5% per cell. Normalised expression data of filtered cells were subsequently performed for cell clustering and TSNE dimensional reduction. Sixteen clusters were finally established by FindClusters R-function. Each cluster was further annotated by SingleR R-package. Gene signatures per cluster, representing

different TME cells, were further determined by FindAllMarkers R-function. We chose the genes that cater for the threshold of LogFC >1 and adjusted *P*-value <0.05 as the signature of each cell type.

Establishment of various gene signatures

The gene sets representing different types of signatures were acquired from the respective channels mentioned above. For the xCell signature, the score per signature was calculated by the xCellAnalysis function from the R-package. The other gene sets were submitted to the gene set variation analysis (GSVA) R-package to estimate the activity score of different terms based on single sample gene set variation analysis (ssGSEA). The relationship between the gene expression and score per signature was estimated by calculating the Pearson correlation coefficient (PCC). The $|PCC| > 0.3$ and adjusted *P*-value <0.05 were considered moderately correlated. The $|PCC| > 0.6$ and adjusted *P*-value <0.05 were considered as highly correlated.

Determination of Pubtator score and drug target development level of genes

The pubtator score, which was used to define the levels of study for each FRG, was obtained from the Target Central Resource Database (TCRD) (http://juniper.health.unm.edu/tcrd/); we regarded the gene with a score <100 as understudied. To define the drug target development level (TDL) of each FRG, we also referred to the TCRD, which is a public resource produced by the Illuminating the Druggable Genome Knowledge Management Centre (IDG-KMC)/NIH[60]. In accordance of the perspectives of clinical, chemical, and biological activities, TDL was divorced into four categories, that are: 1) Tclin: proteins targeted by approved drugs with known mechanism of action; 2) Tchem: proteins with the shortage of approved drugs but have activities in Guide to Pharmacology, DrugCentral, or ChEMBL and the bioactivities of them match the Activity Threshold confined by TCRD; 3) Tbio: targets that do not have known small molecule activities that match the activity threshold or approved drug, but either beyond the threshold of criteria for Tdark or could be annotated by biological process or molecular function leaf term (s) from gene ontology (GO) with an experimental evidence code; 4) Tdark: proteins which are studied by very few researcher and do not match standard mentioned above but satisfy two or more of the following filtering criteria, that are, i) A PubMed text-mining score from Jensen Lab <5; ii) ≤ 3 Gene RIFs; iii) ≤ 50 antibodies available according to antibodypedia website (http://antibodypedia.com).

Gene dependency score (gDS) analysis

To evaluate the 'essential' of each FRG in bladder cancer, we engaged the gDS from previous research[50]. The lower gDS per gene is accompanied by more importance for tumour cells. gDS <-1 indicates that gene loss is lethal for tumour cells, and gDS amid -1 and 0 illustrates that gene deletion affects cells viability to some degree. On the other hand, gDS >0 represents a gene that does not affect cell viability when depleted.

Differential expression analysis and protein expression validation

The whole genome expression profile of TCGA-BLCA was used to conduct differential expression analysis, and the results about FRG were obtained. The analysis was based on the limma R-package from the Bioconductor (https://www.bioconductor.org/). Benjamini–Hochberg method was performed to adjust the *P*-value to control the false discovery rate (FDR). To explore the distribution of FRG in bladder cancer, we referred to the immunohistochemistry data from the human protein atlas (HPA) database (https://www.proteinatlas.org/), which contained large-scale of protein data covering 44 human tissues and 15 323 genes. From this, the protein expression situation of each FRG on bladder cancer could be determined.

Prognosis-related genes analysis and survival curve

mRNA expression per gene was matched with clinical overall survival data, and the univariate Cox regression analysis was performed. Hazard ratio (HR) and *P*-value were used to describe the correlation between gene and prognosis (i.e. a gene with HR >1 and *P*-value <0.05 suggests the gene is a risky factor for prognosis). Then, the ideal cut-off of expression value per gene was determined by surv_cutpoint R-function to divorce the data into the high-/low-expression cohort, and Kaplain–Meier survival curves were depicted to demonstrate the prognostic difference between the two groups based on survminer and survival R-package. The difference in OS between cohorts was tested using the log-rank test.

FRG index (FRGI) and nomogram establishment

By integrating mRNA expression profiling of prognosis-related FRG, a novel computational framework was utilised to identify a fibroblast-related gene signature using a couple of machine learning algorithms. The prognosis-related FRG identified by univariate Cox regression analysis was presented to 10 machine learning algorithms, including stepwise Cox, CoxBoost, elastic network (Enet), Ridge regression, Lasso, random survival forest (RSF), partial least squares regression for Cox (plsRcox), generalised boosted regression modelling (GBM), Boruta, and pamr on the basis of 10-fold cross-validation were further used to screen out the most valuable FRG signature by overlapping their results. The screened FRG signature was further proceeded to conduct multivariate Cox regression, and the FRGI was finally established:

$$\mathrm{FRGI} = \sum_{i}^{n} \mathrm{FRG}_i * \mathrm{Coef}_i$$

For each patient, *n* is the number of prognostic FRG, FRGi is the mRNA expression of FRG, and Coefi is the regression coefficient.

Then, the FRGI was validated by datasets representing bladder cancer and other types of cancer by analysing the predicted effect of FRGI on prognosis (i.e. overall survival and recurrence-free survival) and the relation between FRGI and other clinical variables. Furthermore, datasets representing bladder cancer were further classified into different clinical subgroups (i.e. according to age, data was divorced into age >60 and age ≤ 60 groups) to validate the robustness of FRGI. The FRGI and other clinical

variables associated with prognosis were further utilised to construct a nomogram to predict the OS rate or RFS rate of 1-/3-/5 years in different bladder cancer datasets. Then, the ROC curve, calibration, decision curve analysis (DCA), and survival curve were performed to evaluate the predicted efficacy of the nomogram model on prognosis. Then, the data across cancer types downloaded from the TCGA, ICGC, and GEO mentioned above were conducted for further validation.

Finally, the FRG mRNA expression from bladder cancer datasets was conducted with unsupervised clustering utilising the factoextra R-package. From this, the Euclidean distance per sample was calculated, and then the hierarchical cluster was conducted by applying the ward.D2 method. Ultimately, BLCA datasets were stratified into two clusters, including FRG hot (subtype with high-expression of FRG) and FRG cold (subtype with low-expression of FRG) types. Established subtypes were matched clinical variables (i.e. pathologic stage, grade, age, sex, etc.) to explore their distribution across subtypes based on a χ^2 test.

Mechanism analysis

For the GSEA method, the whole genome expression profile was ordered by FRG subtype, and then the data and cancer-related hallmark gene sets downloaded from the Molecular Signatures Database (https://www.gsea-msigdb.org/gsea/msigdb/index.jsp) was submitted to GSEA software. The top 20 pathways highly enriched in fibroblast hot type were demonstrated by barplot. Then, we merged all the results generated from five datasets representing bladder cancer to explore the recurring enrichment pathways. For GSVA, mRNA expression profile and hallmark gene sets were submitted to the GSVA R-package, and then pathway activity per sample was calculated. Pearson method was performed to reveal a correlation between pathway activity and FRGI, and the significance was demonstrated by the function as follows:

$$\text{Sigificance} = -\log_{10}(\text{FDR})$$

For GSA, each mRNA dataset was presented to the GSA R-package to compare the differential expression of gene sets in each subtype relative to the others (parameters: response type use 'two-class unpaired', FDR is 0.2, while others are default). The method returns score and *P*-values to assess the significance of lower or higher expression of the gene set between two groups. We generate a significant score to show and depict conveniently the significant enrichment pathways by the function:

$$\text{Significance} = -\log_{10}(\text{P} - \text{value}_i) * \text{Score}_i * 0.1$$

The i indicates each significant pathway, and 0.1 is a weighted coefficient to keep the function from generating a larger span of the significance score.

Cross-talk and mechanism among FRG

For each FRG, we depicted their co-expression situation by calculating the Pearson correlation coefficient (PCC) using the Pearson method from the Hmisc R-package. Then, FRG were submitted to the public PPI network website (https://string-db.org/) to explore their protein interaction situation. Then, the FRG were presented to The database for annotation, visualisation, and integrated discovery (DAVID) datasets (https://david.ncifcrf.gov/) to analyse their potential mechanism; the top 10 significant items were demonstrated by barplot.

Copy number variation and mutation characterisation

To characterize the mutation condition of FRG or FRG subtype, we downloaded the simple nucleotide variation data of TCGA-BLCA by utilising the GDCquery function in the TCGAbiolinks R-package. The mutation condition and plot were analysed and depicted using the maftools R-package. To estimate the recurrent focal SCNA, we obtained the segmentation files of TCGA-BLCA tumour samples from the TCGA GDC Data Portal (https://portal.gdc.cancer.gov). Then, we identified the significantly recurrent focal genomic regions of BLCA and subtypes by presenting the CNA data to the genomic identification of significant targets in cancer (GISTIC 2.0) algorithm from the public website - pattern (https://cloud.genepattern.org/gp/pages/index.jsf). We utilised the parameters, including a 0.99 confidence level and *q*-value <0.25. According to the threshold of GISTIC amplitude, four types of CNA of the sample with significant focal events were determined, including deletion (shallow and deep deletion) and amplification (low-level and high-level amplification).

Immune infiltration and immune therapeutic response analysis

The xCell R-package was utilised to explore the infiltration levels of immune cells, immune score, stromal score, and microenvironment score. The percentage of 22 types of immune cells per sample was calculated by cell type identification by estimating relative subsets of rna transcripts (CIBERSORT). The TIDE method was used to explore the immune therapeutic response based on a public website (http://tide.dfci.harvard.edu). Other immune therapeutic response datasets were downloaded from their corresponding channel to explore the relationship between FRGI, immune therapeutic response, and prognosis.

Statistical analysis

All analyses in this study were performed using R software. The unpaired *t*-test was employed to evaluate the mean value differences between the two groups. The log-rank test was utilised to assess the relationship between variables and the prognosis. The χ^2 test was conducted on contingency table data to depict the distribution distinction. The Pearson method was used to estimate the relation between the two groups. **P*-value <0.05; ***P*-value <0.01; ****P*-value <0.001; *****P*-value <0.0001; ns, no significance.

Discussion

MIBC accounts for nearly 25% of all BLCA patients; most of them are locally advanced or metastatic at diagnosis, which is always associated with poor prognosis, requiring systematic treatment[4]. However, due to the heterogeneity of BLCA, conventional treatment methods are always limited, thus causing unsatisfactory clinical outcomes. Research has been reported that molecular cancer of bladder cancer is associated with prognosis and therapeutic efficacy[8,61]. Despite the molecular characterisation of bladder cancer, TME is also essential and closely related to bladder cancer malignancy, recurrence potential, and

therapeutic response[62–64]. Therefore, exploiting and understanding the functions and mechanisms of characterisation of the various components of the TME is mainly essential for revealing the mechanisms of BLCA recurrence and developing novel therapeutic strategies against BLCA.

By analysing the TME from the scRNA-seq data, which comes from BLCA tissues representing different T stages, we found that the distribution of fibroblasts and endothelial cells is primarily associated with the bladder cancer T stage. We took great interest in fibroblasts due to their complex functions on tumours and little research on bladder cancer. Fifty-four fibroblast-derived genes that were identified, other scRNA-seq datasets and TME signatures from bulk RNA sequences were utilised to validate the screened genes. By presenting the mRNA expression data of FRG to machine learning algorithms in the TCGA-BLCA dataset, three core FRG (FN1, CRYAB, and COL6A1) are finally determined to construct risk signature (FRGI) on predicting prognosis. Furthermore, the risk signature was subsequently validated from four other external BLCA cohorts (GSE13507, GSE31684, GSE32894, and IMvigor_120) and other cohorts representing different types of cancer. The results indicate that the FRGI was practical in predicting the prognosis of BLCA. Then, a nomogram including clinical characteristics and FRGI was constructed, and the results revealed that it worked well in predicting overall survival and recurrence-free survival. FN1 has been found to derive from fibroblast and has all sorts of functions in regulating bladder cancer. FN1, located in senescence-like fibroblasts, has been found preferentially enriched in metastatic lesions and promotes gallbladder carcinoma (GBC) migration and invasion[65]. Other research indicated that FN1 derived from CAF could promote progression through the JUN-Hippo signalling pathway in hepatocellular carcinoma[66]. In vitro cellular models, CAF-conditioned media, and recombinant FN1 could facilitate the migration and invasion of glioblastoma cells[67]. Targeting FN1 could reverse mesenchymal morphology, inhibit cell migration and invasion, and sensitise breast cells to doxorubicin[68]. In addition, comprehensive bioinformatic analysis also reveals that FN1 acts as a CAF marker, which correlates with prognosis and TME in gastric cancer, clear cell renal cell carcinoma, and prostate cancer[69–71]. COL6A1 is also found to be dysfunctional in many malignancies, which has been observed in all CAF subtypes[72]. In osteosarcoma (OS), overexpression of COL6A1 could convert normal fibroblasts to CAFs by secreting several proinflammatory cytokines, such as IL-8 and IL-6. The activated CAFs could facilitate OS cell migration and invasion by regulating the TGF-β/COL6A1 signalling pathway; these results revealed there is a close relation between COL6A1, fibroblasts, and cancer[73]. In contrast to FN1 and COL6A1, very little evidence indicates a relationship between CRYAB, fibroblasts, and cancer. In cardiac fibrosis, LBH could up-regulate CRYAB, mediating TGF-β1-induced fibroblast-to-myofibroblast transition and EMT-like processes[74]. Much research reveals that CRYAB participates in cancer development and metastasis[75–77]. However, whether CRYAB impacts bladder cancer by mediating CAFs still needs further experimental evidence. Considering these three genes' function and gDS score on tumours, especially FN1, which has been developed as a small molecular inhibitor, we suspected that targeting them could mediate CAFs to play a role of antitumour. We further divorced the BLCA into two subtypes based on the expression of FRG, and conducted mechanism analyses. In the FRG hot type, multiple pathways occur in recurrent alteration. It could be suspected that these FRG signatures might activate these pathways to promote tumour progression in bladder cancer, which still needs further validation.

Besides predicting prognosis, it has been known that there is a relationship between fibroblast and therapeutic response[31,33,35]. As expected, high FRGI reveals worse chemotherapy and immune therapeutic outcomes, suggesting that CAF infiltration could prevent tumours from therapy. In triple-negative breast cancer (TNBC), it has been uncovered that inhibiting FN1 expression could induce apoptosis and resensitization to chemotherapy[78]. Recent research reveals that FN1 expression is a predictive biomarker in some patients with chemotherapy-resistant RCC, which is especially related to two RCC cell lines with starvation resistance[79]. Even though no research reveals whether FN1 has a therapeutic effect on bladder cancer, comprehensive bioinformatics research has regarded FN1 as a highly precise predictive biomarker for the responses to immunotherapy and chemotherapy[80,81]. Rainer Witting *et al.*[82] reported a study that was performed to identify candidate genes for drug resistance based on drug-sensitive human malignancy melanoma cell line and revealed that CRYAB was one of the strongest candidates for resistance against DNA-damaging drugs, such as cisplatin, etoposide, and fotemustine. In TNBC cells with CRYAB expression, wound healing assay revealed that fluorouracil (5-FU), typical chemotherapy for treating TNBC, significantly increased cell motility, which could be reversed by siRNA targeting CRYAB, revealing that these gene targeting could be a supporting treatment combined with first-line therapy[83]. However, in bladder cancer, the role of CRYAB seems to appear to have adverse results[84]. Apparently, this controversial gene still needs to be further explored by subsequent preclinical trials. Another predicted model revealed that COL6A1 was a hub-gene that correlates with prognosis and immune therapeutic response in bladder cancer[85]. COL6A1 was also identified as a top candidate with potential predictive value in determining cisplatin response or not as a noninvasive biomarker in nonsmall cell lung cancer[86]. Nevertheless, the role of fibroblast-derived COL6A1 on bladder cancer remains unclear and needs further excavation.

Tumour cells can survive because the TME allows them to escape immune surveillance and drug interference[87]. Though FRGI and FRG subtypes could be effective predictive methods on immunotherapeutic response in bladder cancer, the TME components were complicated, indicating that a single predicting model based on a single element is one-sided. So, we pay more attention to other ingredients in TME. As a type of protumour immune in TME, we observed multiple protumour immune cells highly activated in high FRGI or FRG-hot types, such as Tregs and macrophage M2. Tregs are found to inhibit effector T-cell proliferation and cytokine production, thus suppressing immune-mediated inflammation and causing poor outcomes of patients' survival[88,89]. Evidence from clinical and experimental studies has pointed out that tumour-associated macrophages (TAMs) promote cancer metastasis by releasing a series of cytokines, such as inflammatory factors, growth factors, and chemokines[90–92]. M2 macrophages have been found to inhibit inflammatory responses and promote angiogenesis and tissue repair and remodelling[93]. So, it could be deduced that FRG could activate or cooperate with these protumour immune cells to play a role in immune suppression.

So far, immunotherapy research has mainly focused on T-cells[94]. The outcomes of patients with tumours are quite associated with cooperation in both antitumour and protumour

immune in TME. Thus, we concentrate on antitumour immunity. Intriguingly, B cells also show a high activity in high FRGI groups. Considering that B cells, which act as antigen-presenting cells, send antigen to T-cells, we speculated that activation of B cells in the high FRGI group might be compensatory. Interestingly, we found CD4 + T-cells, CD8 + T-cells, and NKT show no significant alteration in high or low FRGI groups. Considering that CD8 + T-cells are stable in function and regarded as a marker of 'cold' and 'hot' tumours[55], we further considered CD8 + T-cells to be representative antitumour immune cells for further research. As we expected, in patients with low CD8 + T-cell activity, high fibroblast infiltration always causes poor prognosis and immunotherapeutic response, indicating that fibroblast infiltration does sometimes conspire to inhibit CD8 + T-cell activity. However, whether the inhibition is direct or not is still unclear and requires further exploration. Combining CD8 + T-cells activity and FRG subtype could enhance the prediction efficacy of the immune therapeutic response, revealing that the immune response is caused by crosstalk between the antitumour and protumour immune systems. We finally featured the four subtypes by conjugating pathway and TME signature, copy number variation, and single nucleotide variation. For instance, the CD8-FH type is characterised by EMT and apical junction pathways enrichment. CD8-FC type is enriched by tumour proliferation rate, E2F target, G2M checkpoint, cell cycle activity, and DNA repair. Antitumour immune cells, IL6 JAK STAT3 signalling, IL2 STAT5 signalling, complement highly enriched in CD8 + FH type. At the same time, the CD8 + FC type features a high antitumour immune signature and a low protumour immune signature. All in all, these novel enrichment results provided an orientation about specialized treatment strategies for each subtype.

Although our FRGI and correspondent subtypes showed excellent performance in multiple cohorts representing bladder cancer, some inevitable limitations still exist. First, these datasets were retrospectively recruited, which may, to varying degrees, inevitably lead to bias. Second, there is a shortage of clinical phase 3 randomized controlled trials to verify patients' prognosis and therapeutic responses based on determined FRG subtypes. Third, the potential mechanism and biological functions of selected FRG based on bulk datasets and machine learning have not been investigated in bladder cancer cells, which might be necessary for further exploration by experimental research.

In conclusion, we identified three potentially important fibroblast-related genes by combining scRNA and bulk RNA sequence datasets based on machine learning and further constructed FRG subtypes by combining antitumour immune CD8 + T-cells to predict prognosis and immune therapeutic response in bladder cancer; we wished these organised data could be used on further clinical trials and experimental research to explore the practicality and potential mechanism of FRG on bladder cancer.

Ethical approval

Not applicable, all data are obtained from public database, and we do not generate new data.

Consent

Not applicable.

Sources of funding

This work was supported by The National Natural Science Foundation of China (No. 22076138) and Tianjin Science and Technology planning project (NO. 21JCYBJC01750).

Author contribution

E.D., S.L., J.L., and Z.Z.: contributed to the study design; J.L., Z.K., Y.Q., Q.S., and W.W.: collected data and contributed to the bioinformatics analyses; E.D., S.L., and Z.Z.: directed the study, obtained funding, and revised the manuscript; J.L., Z.K., Y.Q., W.W., and W.H.: wrote the manuscript. All authors read and approved the final manuscript.

Conflicts of interest disclosure

The authors declares no conflicts of interest.

Research registration unique identifying number (UIN)

The research has registered at www.researchregistry.com (Unique identifying number: researchregistry10084).

Guarantor

Zhihong Zhang, Shuai Li, and E. Du.

Data availability statement

All data generated or analysed during this study were included in this article. The datasets used and analysed in the current study are available from the corresponding author upon reasonable request.

Provenance and peer review

Not commissioned, externally peer-reviewed.

References

[1] Antoni S, Ferlay J, Soerjomataram I, *et al*. Bladder cancer incidence and mortality: a global overview and recent trends. Eur Urol 2017;71:96–108.
[2] Bhanvadia S. Bladder cancer survivorship. Curr Urol Rep 2018;19:111.
[3] Martinez Rodriguez R, Buisan Rueda O, Ibarz L. Bladder cancer: present and future. Med Clin (Barc) 2017;149:449–55.
[4] Kamat A, Hahn N, Efstathiou J, *et al*. Bladder cancer. Lancet 2016;388:2796–810.
[5] Dobruch J, Oszczudłowski M. Bladder cancer: current challenges and future directions. Medicina (Kaunas) 2021;57:749.
[6] Ho P, Willis D, Patil J, *et al*. Outcome of patients with clinically node-positive bladder cancer undergoing consolidative surgery after preoperative chemotherapy: The M.D. Anderson Cancer Center Experience. Urol Oncol 2016;34:59.e1–8.
[7] Galsky M, Arija J, Bamias A, *et al*. Atezolizumab with or without chemotherapy in metastatic urothelial cancer (IMvigor130): a multicentre, randomised, placebo-controlled phase 3 trial. Lancet 2020;395:1547–57.
[8] Kamoun A, de Reyniès A, Allory Y, *et al*. A consensus molecular classification of muscle-invasive bladder cancer. Eur Urol 2020;77:420–33.
[9] Seiler R, Ashab H, Erho N, *et al*. Impact of molecular subtypes in muscle-invasive bladder cancer on predicting response and survival after neoadjuvant chemotherapy. Eur Urol 2017;72:544–54.

[10] Babjuk M, Burger M, Compérat E, *et al*. European association of urology guidelines on non-muscle-invasive bladder cancer (TaT1 and Carcinoma In Situ) - 2019 Update. Eur Urol 2019;76:639–57.
[11] Driskell R, Lichtenberger B, Hoste E, *et al*. Distinct fibroblast lineages determine dermal architecture in skin development and repair. Nature 2013;504:277–81.
[12] Arina A, Idel C, Hyjek E, *et al*. tumour-associated fibroblasts predominantly come from local and not circulating precursors. Proc Natl Acad Sci USA 2016;113:7551–6.
[13] Rognoni E, Pisco A, Hiratsuka T, *et al*. Fibroblast state switching orchestrates dermal maturation and wound healing. Mol Syst Biol 2018; 14:e8174.
[14] Tomasek J, Gabbiani G, Hinz B, *et al*. Myofibroblasts and mechano-regulation of connective tissue remodelling. Nat Rev Mol Cell Biol 2002; 3:349–63.
[15] Kuzet S, Gaggioli C. Fibroblast activation in cancer: when seed fertilizes soil. Cell Tissue Res 2016;365:607–19.
[16] Erez N, Truitt M, Olson P, *et al*. Cancer-associated fibroblasts are activated in incipient neoplasia to orchestrate tumour-promoting inflammation in an NF-kappaB-dependent manner. Cancer cell 2010;17: 135–47.
[17] Shi X, Young C, Zhou H, *et al*. Transforming growth factor-β signalling in fibrotic diseases and cancer-associated fibroblasts. Biomolecules 2020; 10:1666.
[18] Li Y, Tao Y, Gao S, *et al*. Cancer-associated fibroblasts contribute to oral cancer cells proliferation and metastasis via exosome-mediated paracrine miR-34a-5p. EBioMedicine 2018;36:209–20.
[19] Li H, Zhang Q, Wu Q, *et al*. Interleukin-22 secreted by cancer-associated fibroblasts regulates the proliferation and metastasis of lung cancer cells via the PI3K-Akt-mTOR signalling pathway. Am J Transl Res 2019; 11:4077–88.
[20] Pang T, Yin X, Luo T, *et al*. Cancer-associated fibroblasts promote malignancy of gastric cancer cells via Nodal signalling. Cell Biochem Funct 2020;38:4–11.
[21] Neufert C, Becker C, Türeci Ö, *et al*. tumour fibroblast-derived epiregulin promotes growth of colitis-associated neoplasms through ERK. J Clin Invest 2013;123:1428–43.
[22] Subramaniam K, Tham S, Mohamed Z, *et al*. Cancer-associated fibroblasts promote proliferation of endometrial cancer cells. PloS one 2013;8: e68923.
[23] Du Y, Shao H, Moller M, *et al*. Intracellular Notch1 signalling in cancer-associated fibroblasts dictates the plasticity and stemness of melanoma stem/initiating cells. Stem Cells 2019;37:865–75.
[24] Chong Y, Tang D, Xiong Q, *et al*. Galectin-1 from cancer-associated fibroblasts induces epithelial-mesenchymal transition through β1 integrin-mediated upregulation of Gli1 in gastric cancer. J Exp Clin Cancer Res 2016;35:175.
[25] Radhakrishnan R, Ha J, Jayaraman M, *et al*. Ovarian cancer cell-derived lysophosphatidic acid induces glycolytic shift and cancer-associated fibroblast-phenotype in normal and peritumoural fibroblasts. Cancer Lett 2019;442:464–74.
[26] Erez N, Glanz S, Raz Y, *et al*. Cancer associated fibroblasts express pro-inflammatory factors in human breast and ovarian tumours. Biochem Biophys Res Commun 2013;437:397–402.
[27] Zhang Q, Lenardo M, Baltimore D. 30 Years of NF-κB: a blossoming of relevance to human pathobiology. Cell 2017;168:37–57.
[28] Shen T, Li Y, Zhu S, *et al*. YAP1 plays a key role of the conversion of normal fibroblasts into cancer-associated fibroblasts that contribute to prostate cancer progression. J Exp Clin Cancer Res 2020; 39:36.
[29] Qiao Y, Zhang C, Li A, *et al*. IL6 derived from cancer-associated fibroblasts promotes chemoresistance via CXCR7 in esophageal squamous cell carcinoma. Oncogene 2018;37:873–83.
[30] Inoue S, Ito H, Tsunoda T, *et al*. CD70 expression in tumour-associated fibroblasts predicts worse survival in colorectal cancer patients. Virchows Arch 2019;475:425–34.
[31] Zhang H, Jiang R, Zhou J, *et al*. CTL attenuation regulated by PS1 in cancer-associated fibroblast. Front Immunol 2020;11:999.
[32] Chauhan V, Chen I, Tong R, *et al*. Reprogramming the microenvironment with tumour-selective angiotensin blockers enhances cancer immunotherapy. Proc Natl Acad Sci USA 2019;116:10674–80.
[33] Yan Y, Chen X, Wang X, *et al*. The effects and the mechanisms of autophagy on the cancer-associated fibroblasts in cancer. J Exp Clin Cancer Res 2019;38:171.
[34] Lotti F, Jarrar A, Pai R, *et al*. Chemotherapy activates cancer-associated fibroblasts to maintain colorectal cancer-initiating cells by IL-17A. J Exp Med 2013;210:2851–72.
[35] Garvey C, Lau R, Sanchez A, *et al*. Anti-EGFR therapy induces EGF secretion by cancer-associated fibroblasts to confer colorectal cancer chemoresistance. Cancers 2020;12:1393.
[36] Al-Assar O, Demiciorglu F, Lunardi S, *et al*. Contextual regulation of pancreatic cancer stem cell phenotype and radioresistance by pancreatic stellate cells. Radiother Oncol 2014;111:243–51.
[37] Zhang H, Hua Y, Jiang Z, *et al*. DNM3OSCancer-associated Fibroblast-promoted LncRNA confers radioresistance by regulating DNA damage response in esophageal squamous cell carcinoma. Clin Cancer Res 2019; 25:1989–2000.
[38] Ma Z, Li X, Mao Y, *et al*. Interferon-dependent SLC14A1 cancer-associated fibroblasts promote cancer stemness via WNT5A in bladder cancer. Cancer cell 2022;40:1550–65.e7.
[39] Zhuang J, Shen L, Li M, *et al*. Cancer-associated fibroblast-derived miR-146a-5p generates a niche that promotes bladder cancer stemness and chemoresistance. Cancer Res 2023;83:1611–27.
[40] Feng R, Li Z, Ge G, *et al*. Cancer-associated fibroblast-derived extracellular vesicles mediate immune escape of bladder cancer via PD-L1/PD-1 expression. Endocr Metab Immune Disord Drug Targets 2023;23: 1410–20.
[41] Lazard D, Sastre X, Frid M, *et al*. Expression of smooth muscle-specific proteins in myoepithelium and stromal myofibroblasts of normal and malignant human breast tissue. Proc Natl Acad Sci USA 1993;90: 999–1003.
[42] Affo S, Nair A, Brundu F, *et al*. Promotion of cholangiocarcinoma growth by diverse cancer-associated fibroblast subpopulations. Cancer Cell 2021;39:883.
[43] Chen S, Zhu G, Yang Y, *et al*. Single-cell analysis reveals transcriptomic remodellings in distinct cell types that contribute to human prostate cancer progression. Nat Cell Biol 2021;23:87–98.
[44] Chen H, Yang W, Xue X, *et al*. Integrated analysis revealed an inflammatory cancer-associated fibroblast-based subtypes with promising implications in predicting the prognosis and immunotherapeutic response of bladder cancer patients. Int J Mol Sci 2022;23:15970.
[45] Liu B, Zhan Y, Chen X, *et al*. Weighted gene co-expression network analysis can sort cancer-associated fibroblast-specific markers promoting bladder cancer progression. J Cell Physiol 2021;236:1321–31.
[46] Gu Y, Zhuo H. Identification of a cancer-associated fibroblast signature for predicting prognosis and immunotherapeutic responses in bladder urothelial carcinoma. The Aging Male 2023;26:2233609.
[47] Bagaev A, Kotlov N, Nomie K, *et al*. Conserved pan-cancer microenvironment subtypes predict response to immunotherapy. Cancer Cell 2021;39:845–65.e7.
[48] Aran D, Hu Z, Butte A. xCell: digitally portraying the tissue cellular heterogeneity landscape. Genome Biol 2017;18:220.
[49] Becht E, Giraldo N, Lacroix L, *et al*. Estimating the population abundance of tissue-infiltrating immune and stromal cell populations using gene expression. Genome Biol 2016;17:218.
[50] Tsherniak A, Vazquez F, Montgomery P, *et al*. Defining a cancer dependency map. Cell 2017;170:564–76.e16.
[51] Fu J, Li K, Zhang W, *et al*. Large-scale public data reuse to model immunotherapy response and resistance. Genome Med 2020;12:21.
[52] Thorsson V, Gibbs DL, Brown SD, *et al*. The immune landscape of cancer. Immunity 2018;48:812–830.e814.
[53] Ullman N, Burchard P, Dunne R, *et al*. Cold immunologic strategies in pancreatic cancer: making tumours. J Clin Oncol 2022;40:2789–805.
[54] Ochoa de Olza M, Navarro Rodrigo B, Zimmermann S, *et al*. Turning up the heat on non-immunoreactive tumours: opportunities for clinical development. Lancet Oncol 2020;21:e419–30.
[55] Zhang X, Huang X, Xu J, *et al*. NEK2 inhibition triggers anti-pancreatic cancer immunity by targeting PD-L1. Nat Commun 2021;12: 4536.
[56] Altman DG, McShane LM, Sauerbrei W, *et al*. Reporting recommendations for tumour marker prognostic studies (REMARK): explanation and elaboration. PLoS Med 2012;9:e1001216.
[57] Mariathasan S, Turley S, Nickles D, *et al*. TGFβ attenuates tumour response to PD-L1 blockade by contributing to exclusion of T cells. Nature 2018;554:544–8.
[58] Bindea G, Mlecnik B, Tosolini M, *et al*. Spatiotemporal dynamics of intratumoural immune cells reveal the immune landscape in human cancer. Immunity 2013;39:782–95.

[59] Schubert M, Klinger B, Klünemann M, *et al*. Perturbation-response genes reveal signalling footprints in cancer gene expression. Nat Commun 2018;9:20.
[60] Nguyen D, Mathias S, Bologa C, *et al*. Pharos: collating protein information to shed light on the druggable genome. Nucleic Acids Res 2017; 45:D995–1002.
[61] Sjödahl G, Abrahamsson J, Holmsten K, *et al*. Different responses to neoadjuvant chemotherapy in urothelial carcinoma molecular subtypes. Eur Urol 2022;81:523–32.
[62] Yuan Y, Jiang Y, Sun C, *et al*. Role of the tumour microenvironment in tumour progression and the clinical applications (Review). Oncol Rep 2016;35:2499–515.
[63] Tian Y, Li Q, Yang Z, *et al*. Single-cell transcriptomic profiling reveals the tumour heterogeneity of small-cell lung cancer. Signal Transduct Target Ther 2022;7:346.
[64] Li X, Zhao S, Bian X, *et al*. Signatures of EMT, immunosuppression, and inflammation in primary and recurrent human cutaneous squamous cell carcinoma at single-cell resolution. Theranostics 2022;12:7532–49.
[65] Wang X, Liu C, Chen J, *et al*. Single-cell dissection of remodeled inflammatory ecosystem in primary and metastatic gallbladder carcinoma. Cell Discov 2022;8:101.
[66] Zhang L, Zhang C, Xing Z, *et al*. Fibronectin 1 derived from tumour-associated macrophages and fibroblasts promotes metastasis through the JUN pathway in hepatocellular carcinoma. Int Immunopharmacol 2022; 113:109420.
[67] Galbo P, Madsen A, Liu Y, *et al*. Functional contribution and clinical implication of cancer-associated fibroblasts in glioblastoma. Clin Cancer Res 2024;30:865–76.
[68] Yang X, Hu Q, Hu L, *et al*. miR-200b regulates epithelial-mesenchymal transition of chemo-resistant breast cancer cells by targeting FN1. Discov Med 2017;24:75–85.
[69] Ashok G, Ramaiah S. FN1 and cancer-associated fibroblasts markers influence immune microenvironment in clear cell renal cell carcinoma. J Gene Med 2023;25:e3556.
[70] Ucaryilmaz Metin C, Ozcan G. Comprehensive bioinformatic analysis reveals a cancer-associated fibroblast gene signature as a poor prognostic factor and potential therapeutic target in gastric cancer. BMC Cancer 2022;22:692.
[71] Pan J, Ma Z, Liu B, *et al*. Identification of cancer-associated fibroblasts subtypes in prostate cancer. Front Immunol 2023;14:1133160.
[72] Thorlacius-Ussing J, Jensen C, Nissen N, *et al*. The collagen landscape in cancer: profiling collagens in tumours and in circulation reveals novel markers of cancer-associated fibroblast subtypes. J Pathol 2024;262: 22–36.
[73] Zhang Y, Liu Z, Yang X, *et al*. H3K27 acetylation activated-COL6A1 promotes osteosarcoma lung metastasis by repressing STAT1 and activating pulmonary cancer-associated fibroblasts. Theranostics 2021;11: 1473–92.
[74] Wu A, Zhang L, Chen J, *et al*. Limb-bud and Heart (LBH) mediates proliferation, fibroblast-to-myofibroblast transition and EMT-like processes in cardiac fibroblasts. Mol Cell Biochem 2021;476:2685–701.
[75] Zhu Z, Luo L, Xiang Q, *et al*. MiRNA-671-5p Promotes prostate cancer development and metastasis by targeting NFIA/CRYAB axis. Cell Death Dis 2020;11:949.
[76] Guo Z, Song J, Hao J, *et al*. M2 macrophages promote NSCLC metastasis by upregulating CRYAB. Cell Death Dis 2019;10:377.
[77] Chen D, Cao G, Qiao C, *et al*. Alpha B-crystallin promotes the invasion and metastasis of gastric cancer via NF-κB-induced epithelial-mesenchymal transition. J Cell Mol Med 2018;22:3215–22.
[78] Saatci O, Kaymak A, Raza U, *et al*. Targeting lysyl oxidase (LOX) overcomes chemotherapy resistance in triple negative breast cancer. Nat Commun 2020;11:2416.
[79] Isono T, Suzaki M. Analysis of the characteristics of chemotherapy-resistant renal cell carcinomas based on global transcriptional analysis of their tissues and cell lines. PloS One 2019;14:e0225721.
[80] Zhang X, Liu H, Zhang J, *et al*. Fibronectin-1: a predictive immunotherapy response biomarker for muscle-invasive bladder cancer. Arch Esp Urol 2023;76:70–83.
[81] Chang Z, Li R, Zhang J, *et al*. Distinct immune and inflammatory response patterns contribute to the identification of poor prognosis and advanced clinical characters in bladder cancer patients. Front Immunol 2022;13:1008865.
[82] Wittig R, Nessling M, Will R, *et al*. Candidate genes for cross-resistance against DNA-damaging drugs. Cancer Res 2002;62:6698–705.
[83] Yang L, Haga Y, Nishimura A, *et al*. Fluorouracil exacerbates alpha-crystallin B chain-mediated cell migration in triple-negative breast cancer cell lines. Sci Rep 2023;13:4010.
[84] Ruan H, Li Y, Wang X, *et al*. CRYAB inhibits migration and invasion of bladder cancer cells through the PI3K/AKT and ERK pathways. Jpn J Clin Oncol 2020;50:254–60.
[85] Zhang X, Liu J, Yang X, *et al*. High expression of COL6A1 predicts poor prognosis and response to immunotherapy in bladder cancer. Cell Cycle 2023;22:610–8.
[86] Böttger F, Schaaij-Visser T, de Reus I, *et al*. Proteome analysis of non-small cell lung cancer cell line secretomes and patient sputum reveals biofluid biomarker candidates for cisplatin response prediction. J Proteomics 2019;196:106–19.
[87] Zou Y, Zheng S, Deng X, *et al*. The role of circular RNA CDR1as/ciRS-7 in regulating tumour microenvironment: a pan-cancer analysis. Biomolecules 2019;9:429.
[88] Sakaguchi S. Naturally arising CD4 + regulatory t cells for immunologic self-tolerance and negative control of immune responses. Annu Rev Immunol 2004;22:531–62.
[89] Wang H, Franco F, Ho P. Metabolic regulation of tregs in cancer: opportunities for immunotherapy. Trends Cancer 2017;3: 583–92.
[90] Cho H, Jung J, Lim D, *et al*. Bone marrow-derived, alternatively activated macrophages enhance solid tumour growth and lung metastasis of mammary carcinoma cells in a Balb/C mouse orthotopic model. Breast Cancer Res 2012;14:R81.
[91] Kawata M, Koinuma D, Ogami T, *et al*. TGF-β-induced epithelial-mesenchymal transition of A549 lung adenocarcinoma cells is enhanced by pro-inflammatory cytokines derived from RAW 264.7 macrophage cells. J Biochem 2012;151:205–16.
[92] Chen J, Yao Y, Gong C, *et al*. CCL18 from tumour-associated macrophages promotes breast cancer metastasis via PITPNM3. Cancer Cell 2011;19:541–55.
[93] Sica A, Mantovani A. Macrophage plasticity and polarization: in vivo veritas. J Clin Invest 2012;122:787–95.
[94] Laumont C, Banville A, Gilardi M, *et al*. Tumour-infiltrating B cells: immunological mechanisms, clinical impact and therapeutic opportunities. Nat Rev Cancer 2022;22:414–30.